Analysis of the Dynamic Interferences between the Stator and Rotor of a Refrigeration Compressor Motor

Swen Thompson

Thesis submitted to the Faculty of the Virginia Polytechnic Institute and State University in partial fulfillment of the requirements for the degree of

Master of Science
in
Mechanical Engineering

Dr. Reginald G. Mitchiner, Chairman
Dr. Robert L. West
Dr. Alfred L. Wicks

May 7, 1997
Blacksburg, VA

Keywords: Refrigeration compressor, electric motor, stator/rotor interference, air gap eccentricity, unbalanced magnetic pull, finite element analysis

Analysis of the Dynamic Interferences between the Stator and Rotor of a Refrigeration Compressor Motor

Swen Thompson

(ABSTRACT)

This thesis involves the development and study of a finite element model of a hermetic, single-vane compressor and a single-phase alternating current induction motor assembled in a common housing. The manufacturer of this unit is experiencing a high scrap rate due to interference during operation between the stator and rotor of the motor. The rotor shaft of the motor is non-typical because of its cantilever design. The finite element model was first subjected to eigenvalue analysis. This revealed that the interference producing displacements were not the result of torque application to the rotor at a frequency close to an eigenvalue of the mechanical system. After a review of the literature and discussions with Electrical Engineering Department faculty possessing extensive motor experience, it was surmised that the physical phenomenon causing the rotor displacement was unbalanced magnetic pull. This phenomenon occurs in the air gap of rotating electric machines due to eccentricity in the air gap.

The model was then subjected to simultaneous harmonic force inputs with magnitudes of unity on the rotor and stator surfaces to simulate the presence of unbalanced magnetic pull. It was found that the rotor shaft acts as a cantilever beam while the stator and housing are essentially rigid. The displacements due to these forces were examined and then scaled to develop the motor parameters necessary to produce the radial forces required for stator/rotor interference. Several recommendations were then made regarding possible solutions to the interference problem.

Acknowledgements

The author wishes to thank his committee chairman Dr. Reginald G. Mitchiner for his support and guidance in the development of this thesis. The author also wishes to thank professors R.L. West and A.L. Wicks for their contributions to this project. The author wishes to send his gratitude to Dr. Jaime De La Ree Lopez of the Bradley Department of Electrical Engineering for his guidance with the electrical engineering portions of this project.

The author's sincerest gratitude goes out to his family for their continued support throughout his academic career. Without this support his success would have not been possible.

The author would like to thank Mrs. Jan Riess and Mr. Ben Poe for their help with all of the day to day problems of graduate school. The author would also like to thank his office mates and friends for their encouragement during the pursuit of his master's degree.

Table of Contents

List of Illustrations

List of Tables

Chapter 1.0 Introduction

Electric motors are essential in today's society. These devices power everything from small household appliances to large industrial processing equipment, and their potential applications continue to grow. One such application for electric motors is as the power input for refrigeration compressors. The object of this study is the analysis of such an application. The compressor and motor in question are employed in a combination unit currently produced by the Tecumseh Products Company for use in applications such as larger office-type water coolers and medium-sized refrigeration units. A high percentage of these motors are experiencing interference problems during running conditions, resulting in a high scrap rate for the manufacturer. There were two goals established for this study. The first goal was to model as accurately as practical the physical aspects of this unit and to determine the mechanical response of the system due to force inputs characteristic of those encountered during operating conditions. The second goal was to use the results of the study to make suggestions to the manufacturer regarding potential design modifications to eliminate the interference problem.

The compressor/motor unit is modeled using the finite element method (FEM). This method was required due to the lack of closed form solutions for the geometry of the compressor components. It was initially known that the interference encountered during operation was a radial displacement of the rotor larger than the stator/rotor air gap. It was felt that the ability to reproduce the magnitude of this interference for visual inspection with the software was of prime importance and much effort was put towards making this possible.

The forcing functions used in predicting the component displacements were typical of those resulting from the air gap eccentricity that can occur in an electric motor. The nature of these forces was determined by other investigators. The true magnitudes of the forcing functions were not determined. Instead, the magnitude of unity was used for the analysis. This approach yielded a set of displacements that may be scaled accordingly.

The study is organized into several chapters. Chapter 2 presents the review of the technical literature for the study. Chapter 3 presents the background of the motor and the interference problem. Chapter 4 presents the modeling approach used for the FEM analysis, including all simplifications. Chapter 5 presents the results of the FEM analysis. Chapter 6 presents all conclusions from the study and areas to be considered for future investigations.

Chapter 2.0 Literature Review

Much information is available in the technical literature regarding dynamic interferences, which are commonly referred to as bumping, between the rotor and housing of turbomachinery. However, this information is heavily biased towards such issues as the physics associated with the component contact and the effects of degradation problems such as excessively worn bearings and loose rotor blades. Since the system under study utilizes all new components it was decided that these findings were not relevant to this analysis.

Several references exist in the literature dating from the 1910's through the 1960's regarding air gap eccentricity in induction machines and one of its fundamental consequences - unbalanced magnetic pull (u.m.p.). However, the theories behind many of these references are unclear and produce no definite conclusions.

In 1974, Rai [1] completed extensive experimental investigations on all aspects of air gap eccentricity in induction motors. These experiments examined both static and dynamic eccentricities on 2-pole motors featuring unslotted, wound and cage rotors. These experiments consisted of extensive measurements of eccentricity fields, air gap flux density, unbalanced magnetic pull, vibratory forces, losses and torque under various operating conditions from no-load to full-load and during starting. In this work it was determined that the following driving forces of different frequencies can occur in electrical machines

1) Mechanical unbalance producing driving forces at the frequency of rotation.
2) Inherent magnetic radial forces at twice line frequency.
3) Static eccentricity producing twice line frequency vibratory driving forces.
4) Defective rotor winding producing twice slip frequency vibration.
5) Dynamic eccentricity producing vibratory forces at rotational speed with a modulation at twice slip frequency. In addition, small vibratory forces at line frequency and twice line frequency can occur.
6) Small static eccentricities can produce vibratory forces at line frequency.
7) Stator harmonics can produce radial forces at twice-line frequency.
8) Certain combinations of harmonics cause vibrations at twice slip frequency.

It was reported that in general, a number of these potential driving forces might exist depending on the types of asymmetry present.

In 1989 Timar, Fazekas, Kiss, Miklos and Yang produced a text on noise and vibrations in electrical machines [2]. In the text it was stated that in single-phase asynchronous motors unbalanced magnetic pull can result in the production of a radial forces at angular frequencies of $2f_1$, $2sf_1$, $2(1-s)f_1$, $2(2-s)f_1$, $(3-s)f_1$ and $(1\pm s)f_1$ where f_1 is the line frequency and s is the slip frequency of the rotor. Slip frequency is defined as the frequency of the voltages induced in the rotor due to relative motion between the stator and rotor fields.

In 1994 Ozturk, Balikcioglu, Acikgoz and Bahadir produced a paper on the origins of electromagnetic vibrations in series fractional horsepower motors [3]. This paper summarized the works of Rai, Timar, and others with respect to unbalanced magnetic pull and the resultant forces. In their research the authors used radial forces due to static eccentricity occurring at twice the voltage supply frequency and radial forces due to dynamic eccentricity occurring at rotational frequency. The concept of static and dynamic eccentricities will be discussed in Chapter 2.

The final area explored in the literature was the effect of laminations used in the construction of the stator and rotor. In 1979 Girgis and Verma [4] determined that the laminated construction of stators has virtually no effect on the location of natural frequencies. However, laminations cause a significant damping in amplitudes of vibration and thus must be taken into consideration when performing stator analysis.

Chapter 3.0 Problem background

3.1 Motor/compressor design

The compressor/motor unit in question for this study consists of a hermetic, single-vane compressor and a four-pole single-phase alternating current (AC) induction motor that operates at 1750 rpm. These two components share a common housing, as shown Figure 1. The assembly consists of the following eight major components - the lower housing, upper housing, stator, rotor, rotor shaft, upper support collar, compression chamber and lower support collar. The compressor charge is drawn through the port at the top of the unit, down the inlet tube, through the center hole in the rotor shaft and into the chamber for compression. After compression, the charge is exhausted through a discharge tube and out of the port on the side of the lower housing.

While the bearings are not shown in Figure 1, it can be seen that the rotor shaft for the electric motor is supported by bearings at the compression chamber only. In other words, the rotor shaft is of a cantilever design. This is in contrast to most electric motors, which utilize a bearing support on each end of the shaft. The purpose of the cantilever approach is to minimize costs. Since this is a very inexpensive unit, the savings involved with the deletion of a second bearing and the associated installation costs are significant.

The compression chamber is a rectangular block of cast iron secured to the lower housing by a press fit. This fit is accomplished by rounding the four corners of the chamber to a slightly larger radius than the inner radius of the lower housing.

The stator is manufactured in the shape of a hexagonal cylinder and is also attached to the lower housing through a press fit. This is again accomplished by rounding the six corners of the stator to a slightly larger radius than the inner radius of the lower housing. The stator consists of multiple thin steel laminations and has copper windings distributed through its slots.

The rotor is of the squirrel cage design and features conducting bars embedded parallel to the axial direction of the rotor. These bars are placed a specified distance below the rotor outer radius. The rotor is also constructed of multiple thin steel laminations, but the conducting bars, end caps, and counter weights are aluminum.

The housing consists of formed steel upper and lower sections. The outer radius of the upper housing is slightly smaller than the inner radius of the lower housing. This allows the upper housing to be inset into the lower housing so that the two components may be joined through a lap weld around the housing perimeter. The lower housing is connected to a mounting surface by a stamped steel plate containing three hole bosses 120° apart.

The rotor shaft and upper and lower support collars used in the unit are constructed of cast iron.

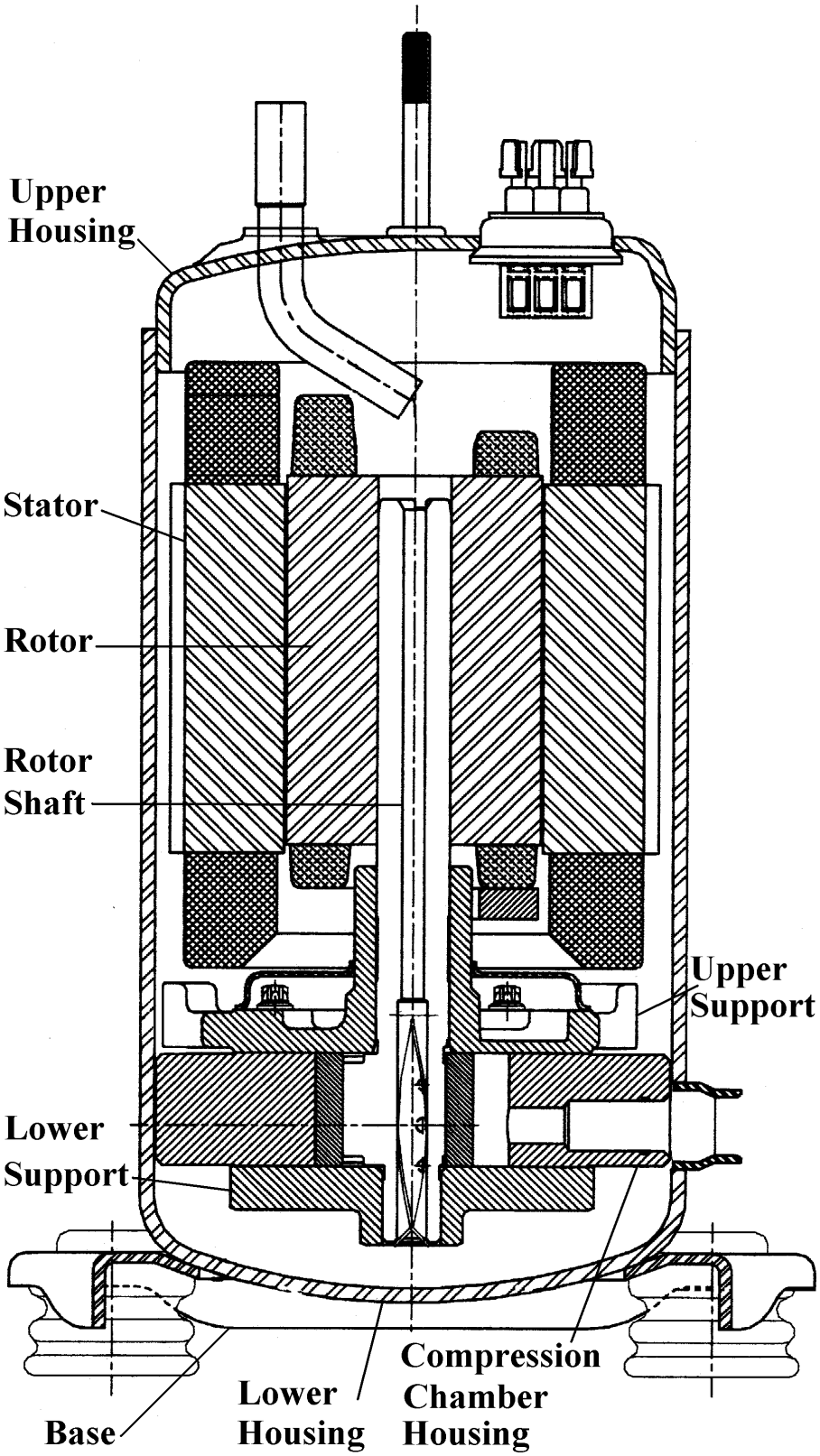

Figure 1. Cross-sectional view of compressor as supplied by the manufacturer

3.2 Interference problem and initial assumptions

As stated earlier the interference experienced during operation occurs between the stator and rotor of the motor. Currently each motor must be tested for this problem as it leaves the assembly line, and approximately thirty-five percent fail.

At the beginning of this analysis the concept of unbalanced magnetic pull was not known to the author. The initial assumption was that the 1750 rpm (29.2 Hz) frequency of the torque applied to the rotor was close to an eigenvalue of one of the assemblies in the system, thus causing random lateral rotor displacements. The most likely culprit in this scenario was thought to be the assembly consisting of the compression chamber, rotor shaft, rotor, and upper and lower support collars. If the actual amount of interference between the components could be accurately determined using finite element analysis, appropriate recommendations for modifications could be made. It was felt that the most likely cure would be to increase the air gap between the stator and the rotor. There would be a practical limit to an air gap increase, however, as this increase has a negative effect on motor output.

3.3 Air gap asymmetries and the resulting forces

As stated in Chapter 2 many works have been published regarding air gap asymmetries and their effects. The discussion of air gap asymmetries and unbalanced magnetic pull presented in this section is a synopsis of the works of Rai [1] and Timar [2].

The main task in creating electromechanical energy conversion by an asynchronous or induction machine is to produce a rotating sinusoidal magnetic field with a pole number $2p$ in the air gap. A magnetic flux is induced in the air gap due to current flowing through the conductors in the slots. These slots break up the uniformity of the air gap. Thus, the gap will change periodically as the relative position of the stator and rotor changes. The total magnetizing current of an induction machine is supplied from the stator (primary winding), and therefore the air gap is designed to be as small as possible. However, even the smallest deviation of the air gap from the shape of a cylindrical sleeve of uniform thickness will result in considerable relative distortion of air gap permeance.

Deviation from a uniform air gap is also highly possible due to tolerances required in the manufacturing process. This non-uniform air gap can result from one or more of the following manufacturing flaws:

1) imperfect centering of the rotor in the stator bore,
2) non-circular stator bore,
3) non-circular rotor and
4) bent shaft.

The first two flaws produce a stationary or static eccentricity in the air gap of an electric machine, while the last two flaws produce a rotating or dynamic eccentricity.

Regardless of whether the air gap eccentricity is static, dynamic or both, the resulting gap will be at a maximum at one point thus producing a minimum flux and a minimum at one point thus producing a maximum flux. A non-uniform flux can result in the following adverse effects:

1) flux harmonics
2) unbalanced magnetic pull
3) noise
4) harmonics in the rotor and stator currents
5) variation in losses and irregular distribution of heat around the stator bore as a result of 1) and 4)
6) variation in torque as a result of 1) and 4), both during starting and steady state conditions.

The effect considered for this study is unbalanced magnetic pull.

As stated, the presence of a magnetic flux in the air gap of an electric machine produces an attractive force between the stator and rotor in the direction of the flux. In an induction machine the sinusoidal flux distribution revolves in the air gap producing a wave of magnetic pull rotating at twice the frequency of the fundamental field. In a system with a uniform air gap no resultant force occurs due to symmetry. When eccentricity is present, however, upon energizing of the stator equal but opposite unilateral magnetic forces acting on the stator and rotor are produced that always act in such a manner as to increase eccentricity. This phenomenon is known as unbalanced magnetic pull (u.m.p.). A graphical representation of the peripheral distribution of unbalanced magnetic pull on the rotor of a rotating electrical machine from Timar [2] is shown in Figure 2. This figure clearly shows the minimum and maximum magnetic field strengths (g) and the resulting radial forces. It is obvious that all force terms perpendicular to the eccentricity (e) cancel. This leaves the force terms parallel to the eccentricity (e), which sum to produce a resultant radial force $F_{resultant}$. An equal but opposite force situation occurs with the stator.

Due to the sinusoidal distribution of flux around the air gap unbalanced magnetic pull due to static eccentricity is generally treated as a harmonic, vibratory, radial force between the rotor and stator for a given operating condition. The frequency of this harmonic force is twice voltage line supply frequency for the following reason. As the magnetic field distribution revolves in the air gap of an induction machine, it passes a given point twice during each cycle of voltage change, once as a flux entering the stator and once as a flux entering the rotor. Since a force of attraction between the stator and rotor occurs regardless of the direction of the flux, the harmonic input must occur at twice the frequency of the applied voltage.

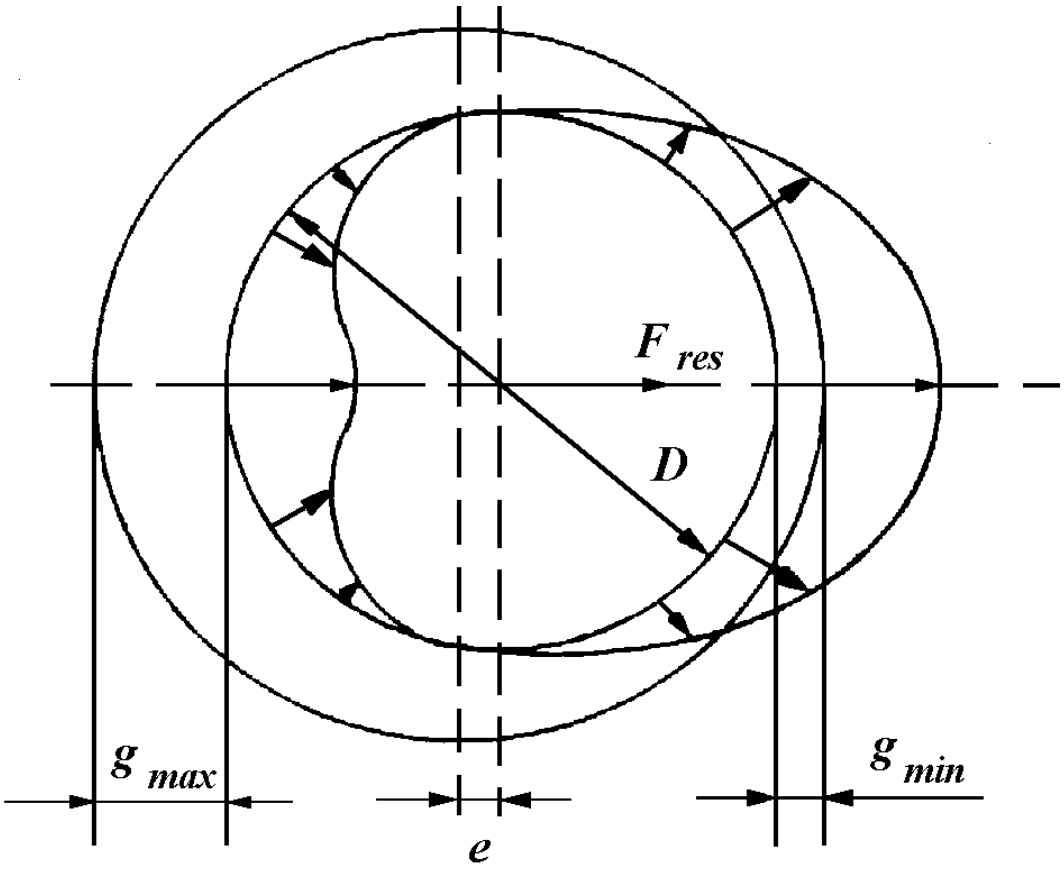

Figure 2. Peripheral distribution of unbalanced magnetic pull

Unbalanced magnetic pull can also arise in electrical machines due to the presence of dynamic eccentricity. This form of unbalanced magnetic pull differs in that it rotates at the rotational speed of the rotor, and thus the effects are similar to those encountered with a mechanical unbalance. This situation can be referred to as magnetic unbalance.

The magnitude and distribution of the forces produced due to unbalanced magnetic pull are dependent upon the distribution of magnetic flux in the air gap. These magnitudes are typically determined by using the Maxwell stress tensor method in conjunction with the finite element method to extract the magnetic flux density in the air gap for a series of static rotor positions. The accurate determination of the flux density is a complicated and crucial step in a complete analysis of an electric motor. Since this phase of the analysis requires a much more extensive electrical engineering background than possessed by the author, it was decided to set the magnitude of the u.m.p. based forces to unity. This approach results in a set of displacements that may be scaled accordingly upon accurate solution of the flux distribution problem.

Ozturk [3] summarized that for analysis purposes the equal but opposite vibratory forces due to unbalanced magnetic pull act upon the stator and rotor of a rotating electric machine. These forces occur at twice the electrical supply frequency for static eccentricity and at the rotor rotational frequency for dynamic eccentricity. If the natural frequency of any part or combination of parts of the mechanical system lies near these forcing frequencies serious vibration problems can result.

Timar [2] defined the relationship between the amplitude of the tangential forces (torque producing forces) and radial forces (i.e., u.m.p. forces) in the air gap as

$$F_{Tangential} = \frac{p\lambda\delta_g}{R} F_{Radial} \tag{3.1}$$

where

p = number of pole pairs
λ = order of the rotor space harmonics
δ_g = geometrical air gap
R = outer radius of the rotor.

The order of the rotor space harmonics for a single-phase AC machine is defined as

$$\lambda = g' S_2 \pm 2g + 1 \tag{3.2}$$

where

$g = 0, \pm 1, \pm 2, \ldots$
g' = negative g
S_2 = number of rotor slots

Normally the ratio of tangential to radial force is considerably less than one. Therefore, it is obvious that the radial force magnitude should be much larger than the tangential.

In summary the presence of eccentricity in the air gap of a rotating electric machine causes equal but opposite harmonic forces of large magnitude at two different forcing frequencies to act upon the stator and rotor at the point of minimum flux density.

Chapter 4.0 Finite element analysis and modeling approach

4.1 Overview of the finite element method

According to Knight [5] the finite element method (FEM) is a numerical method for solving a system of governing equations over the domain of a physical system. The governing equations for FEM are taken from the field of continuum mechanics and the theory of elasticity. While FEM was initially developed for performing structural analysis its use has spread to the fields of heat transfer, fluid mechanics, acoustics, electromagnetics and other areas.

The basis of FEM with respect to structural analysis is summarized in the following steps. The domain of the solid structure under consideration is subdivided into small domains called elements. These elements assemble through interconnection of a finite number of points on each element called nodes. Within the domain of each element a simple general solution to the governing equations is assumed. The specific solution for each element becomes a function of unknown solution values at the nodes. Application of the general solution form to all the elements results in a finite set of algebraic equations to be solved for the unknown nodal values. This subdivision of the structure allows the formulation of equations for each separate element, which are then combined to obtain the solution for the entire system. The structure response can either be linear or non-linear. When the response is linear elastic the algebraic equations are linear and are solved with common numerical procedures. Non-linear solutions are not relevant to this study and will therefore not be discussed.

Due to the division of the continuum domain into finite elements, it is necessary to translate the structure loads and displacement boundary conditions to nodal quantities. Point loads are applied directly to nodes while distributed loads are converted to equivalent nodal values. Boundary conditions such as ground locations are resolved into specified displacements for the specified nodes.

There are two major sources of error associated with the finite element method. The first source of error is the difference between the assumed solution in the element and the exact solution over the domain of the element. The magnitude of this error depends upon the size of the elements in the subdivision relative to the solution variation. Most element formulations converge to the correct solution as the element size is reduced. The second source of error is the precision of the algebraic equation solution. This error is a function of the computer accuracy, the algorithm, the number of equations and the element subdivision. Thus, accurate and efficient representation of the domain of the solid structure is critical.

There are two types of elements available for use in FEM – discrete structural elements and continuum elements. Ideally, all structures should be modeled using three-dimensional continuum

elements. However, this type of element is the most complicated to mesh and hardware and time constraints prohibit its use when other simpler elements will provide adequate solutions.

Structural elements consist of trusses, beams, plates and shells. The formulations of these elements are based upon their respective structural theories. The structural theories of trusses and beams are well accepted and thus the FEM solutions based upon these elements are no more accurate than those resulting from conventional solutions. Plate and shell elements are very much different in that the finite element community has yet to agree on formulations for these elements that produce completely satisfactory results. Therefore, the analyst must exercise great caution when using these elements and should use all means available for verification of the solution.

Continuum elements are two- and three-dimensional solid elements. The formulation of these elements is based upon the theory of elasticity. Few closed form solutions exist for two-dimensional continuum problems, and almost none exist for three-dimensional problems, thus making FEM invaluable.

4.1.1 Finite element solution to time dependent problems

Knight wrote [5] that when inputting an arbitrary time dependent function to a system or structure, a transient response analysis must be performed. The solution to this problem taken by finite element codes is generally one of two types – direct integration or modal superposition.

The integration method involves the direct integration of the system equations after approximation by a finite difference in the time domain for the velocity and acceleration components. This approach involves the total set of system equations and must perform many time steps with a complete solution in each step, thus requiring large computing resources.

The modal superposition method assumes that superposition of the mode shapes corresponding to the lower natural frequencies adequately represents the dynamic response of the structure. The complete response is found by the summation of correct fractions of the low frequency mode shapes. Mathematically this amounts to a transformation of the equations from node displacement coordinates to a set of modal coordinates. The transformation changes the set of system equations consisting of one equation for each degree of freedom in the model to a set of modal equations involving the selected number of mode shapes, thus resulting in fewer equations. While this is an approximation of the total structural response, in most cases it has been shown to be sufficiently accurate.

4.2 Finite element approach

The finite element analysis (FEA) for this study was performed using I-DEAS® Master Series versions 2.1 and 4.0 by the Structural Dynamics Research Corporation (SDRC). The computational hardware used was an IBM RISC 6000 workstation. I-DEAS (Integrated Design Engineering Analysis software) Master Series is a comprehensive software package composed of a number of modules or "applications", each of which are subdivided further into "tasks". The

different applications included in the software are Design, Drafting, Simulation, Test, Manufacturing, Management, and Geometry Translators.

4.2.1 Interference reproduction attempts

At this point an overview of the logic used by the I-DEAS software to transfer information between modules is required. In I-DEAS all components are based upon three-dimensional solid models. These master solid models or "parts" are constructed in the Master Modeler™ task, and from that point the parts serve as the basis for all geometric definitions for all other tasks.

The Master Modeler task contains many capabilities. Included in these are a series of Boolean operators, which allow geometric comparisons between separate parts. These operators are referred to as the Cut, Join and Intersect commands. These allow the designer to manipulate parts that share a common volume in three-dimensional space by

1) removing the common volume from one part and thus creating a new part,
2) joining the two parts at the common volume and thus creating a new larger part and
3) creating a new part which consists only of the common volume between the two parts,

respectively. The purpose of these Boolean operators is to provide the user with the ability to check for static interferences between parts during the design process.

The finite element analysis package in I-DEAS uses a finite element model that is constructed from a part created in the Master Modeler task. It is similar to all other FEA codes in that a finite element mesh is applied to the part geometry (free mesh, mapped mesh, or a manually created mesh), the appropriate boundary conditions and forces are applied and the required analysis is performed (i.e., to determine stress, displacement, temperature, etc.).

It was felt that the most logical approach to the problem at hand would be to create the stator/rotor interference using FEA, and then apply the Intersect command to the deformed finite element model to produce the actual interference. The problem with this approach lies with the distinction made by the software between parts and finite element models. While the finite element model is based upon and, therefore, related to the actual part, the two items are in fact separate entities. This system does not allow the use of Boolean operations on a finite element model. This created a major obstacle because all of the information needed was present, but in an unusable form. It also proved to be an obstacle that consumed a large amount of time because several attempts were made to perform Boolean operations on finite element models before the distinction made between the two was realized.

The initial thought with respect to interference reproduction was that the required information for reconstruction would be contained in the *Simulation Universal Export File*. This file contains all information pertinent to the finite element model, such as the model name, the type of analysis performed, the type of mesh applied, the applied boundary conditions, the eigenvalues of the

system (if calculated), and so forth. The universal export file was desired because all node information for the model (i.e., the node numbers and the original coordinates, the nodal connectivity and the displacements for each node) is also contained in the file. It was felt that this data could be used in conjunction with the Boolean operators to produce the desired interference.

The first attempt was to write the universal file for a displaced shape and then import this file into a new model file. Upon import of this file it was learned that the displaced shape could be imported, but the imported shape was in the form of a finite element model, and no benefits had been realized.

Upon further review of the universal file it was felt that the process of adding the nodal displacements to the original locations was causing the inability to use the Boolean operators on the imported file. Therefore, an external piece of FORTRAN code was developed to retrieve the original node locations and node displacements, sum the two quantities and insert the new locations into the universal file as the original locations. This process also proved to be ineffective because the root of the problem had still not been addressed.

It was at this point that the author realized the true nature of the conflict. The decision was then made to regress to the simplest model possible - a one-element cube - and develop a method to transfer a displaced finite element model into a part.

After further study it was realized that the displaced finite element model could possibly be reconstructed using the nodes on the exterior surface of the model and the various construction commands in the Master Surfacer and the previously described Master Modeler tasks. The primary function of the Master Surfacer task is to allow the designer to create solid models of objects with flowing, sculpted surfaces that would be virtually impossible to create with the Master Modeler. This function is accomplished by either using the solids-based techniques of sweeping and lofting or by creating surfaces from wireframe geometry and assembling these surfaces into a solid part.

The first attempt to reconstruct the displaced model was to draw three-dimensional lines and arcs with the Master Modeler task through the nodes on the surface of the finite element model, therefore, recreating all of the surface features individually. This method proved unsatisfactory because of the poor approximation of the displaced shape between the nodes and the large amount of time required to pick every node on the surface of the finite element model.

The next method attempted was the placing of three-dimensional points through all of the surface nodes of the finite element model and use of the *Surface through Points* command in the Master Surfacer to recreate each individual surface. The individual surfaces could then be fused together using the *Stitch Surfaces* command to create one part. This method was discarded after the initial trial due to its inability to accurately follow the contours of the surface.

The next seemingly plausible solution was to again place three-dimensional points through all of the surface nodes and then to connect all of these points with three-dimensional lines. These lines created the necessary information to allow use of the *Surface by Boundary* command in the Master Surfacer. The intent was to recreate each surface using this command and stitch the surfaces together to form a part. While this method did produce surfaces that accurately followed the contour of each original surface, the resulting surfaces were larger than the designated boundary. An attempt was made to fuse the overlapping surfaces and trim the excess, but stipulations in the program regarding the use of the *Stitch Surfaces* and the *Trim* commands made this path also unfeasible.

It was at this time that the discovery of the *Loft* command in the Master Surfacer Task was made. This command fits a surface through a series of cross-sections in three-dimensional space. It was felt by the author that if the finite element mesh of the rotor was constructed using a mapped mesh scheme with its inherent edge requirements, then a series of wireframes representing cross-sections of the displaced rotor surface could be created with reasonable effort and sufficient accuracy. These cross-sections could then be lofted together to form the associated surfaces, and in turn, the surfaces could be stitched together to form the required part.

This methodology was applied to the simple model of a concentric shaft and tube where each part was treated as a cantilever. An inward radial force was applied to the free end of the shaft to produce a displacement sufficient to cause interference between the shaft and the tube. The displaced finite element model of the shaft was then reconstructed as a part using the lofting procedure. It was found that the cross-sections could not be constructed based upon a full 360° sweep of the local longitudinal axis of the shaft (i.e., the use of one curve to represent the entire circumference of the shaft). This was due to the lack of beginning and ending edges of the surface. However, when the shaft surface was modeled as two halves that could be stitched together (i.e., each half of the total surface was created by performing a 180° sweep of the local longitudinal axis) the procedure worked as desired. This resulted in a part that could then be manipulated with Boolean operators.

4.3 Geometry simplification

Several simplifications were made when modeling the geometry of the various parts. These simplifications were necessary because of the use of mapped meshing and because of the lack of accurate geometric information for some of the components. Had a free mesh been allowable, details such as chamfers and fillets could have been easily modeled, but this was not the case. Since the needed results from the analysis were the natural frequencies and the displacements, the small errors induced by ignoring all chamfers, fillets, and countersinks were deemed inconsequential. The mass and stiffness characteristics of the components were kept as accurate as possible in accordance with the given information.

The greatest simplifications were made to the compression chamber, rotor shaft, lower support and upper support.

The lower support was eliminated entirely. This component added nothing to the assembly in terms of reducing rotor deflection, but it did add significant mass to the system and thus impacted the natural frequencies. The deletion of this part was countered by determining its mass and increasing the density of the compression chamber material by the corresponding amount to result in the same total mass.

The upper support was modified by

1) deleting the flange area and incorporating the mass into the compression chamber housing material, as was done with the lower support. It can be seen in Figure 1 that the cross section of the flange area is not only variable, but is also not symmetric about the hub centerline. This configuration would be virtually impossible to mesh using a mapped meshing scheme. Therefore, an equivalent constant width cross-section for each half was first calculated and then a final constant width cross-section was calculated from the two simplified halves. The mass properties of this final constant thickness flange were then incorporated into the compression chamber housing material by increasing the material density.
2) removing the step in the hub and using the larger of the two hub outer diameters. The hub section of the upper support was assumed to behave as a cantilever beam. From Rao [6] the transverse stiffness of a cantilever beam is defined as

$$K = \frac{3EI}{L^3} \tag{4.1}$$

where

K = stiffness
E = modulus of elasticity
I = area moment of inertia
L = beam length

Since the moment of inertia is a function of the hub diameter, I was calculated using both outer hub diameters. It was found that the ratio of the larger to smaller I values, and thus the stiffness, for the two diameters is 1.61. Since some stiffness was eliminated by ignoring the flange as described in 1) above, it was felt that the use of the stiffer hub section would balance the overall stiffness of the upper support.

The compression chamber housing was modified in that the open area in the chamber itself and the discharge opening were not included (i.e., the chamber housing was modeled as solid minus the center hole for the rotor shaft). These simplifications were made due to the lack of accurate information regarding the chamber area and the small amount of mass that was added with respect to the entire system. As stated above the density of the cast iron material for the compression chamber was increased to account for the eliminated mass of the support collars. The required

increase was calculated to be 149 percent. An isometric view of the compression chamber as modeled is shown in Figure 3. This figure includes the portion of the rotor shaft that is inset in the chamber housing.

The rotor shaft was modified by

1) removing the step in the center hole and using the smaller inner diameter along the entire shaft length. This shaft was also viewed as a cantilever beam with respect to stiffness. Through a comparison of the moment of inertia values, and thus the stiffness, using the two inner diameters it was found that the difference in the *I* values was 1.95 percent. Therefore, a constant inner diameter was deemed appropriate.
2) increasing the overall shaft length to make the shaft end flush with the top end of the rotor. The 3.3 percent increase in shaft mass due to this modification was deemed negligible. Because this additional shaft length is actually inside the rotor (i.e., inside the end mass portion of a cantilever beam with an additional end mass) the change in stiffness is not relevant.

An isometric view of the rotor shaft, upper support and compression chamber housing is shown as modeled Figure 4.

The stator model was modified by neglecting the portion of the copper windings that are outside of the main stator body (i.e., the turns at the ends). Since an actual stator was not available for inspection, the stator from a similarly sized compressor assembly was examined. It was determined that the copper windings account for approximately twenty percent of the total cross-sectional area of the stator. This led to use of stator material properties that were weighted for the eighty percent/twenty percent ratio of steel to copper. The only material properties that were pertinent for this analysis were the modulus of elasticity and the mass density. The stator was also modified by eliminating the rounding of the exterior corners. See Figure 5 for an isometric view of the stator as modeled.

The rotor was modeled in a very similar fashion to the stator. The model did not include the counterweights or the aluminum caps on the ends. The same eighty percent /twenty percent ratio for material properties was used as for the stator, but the ratio was steel to aluminum. See Figure 6 for an isometric view of the rotor as modeled.

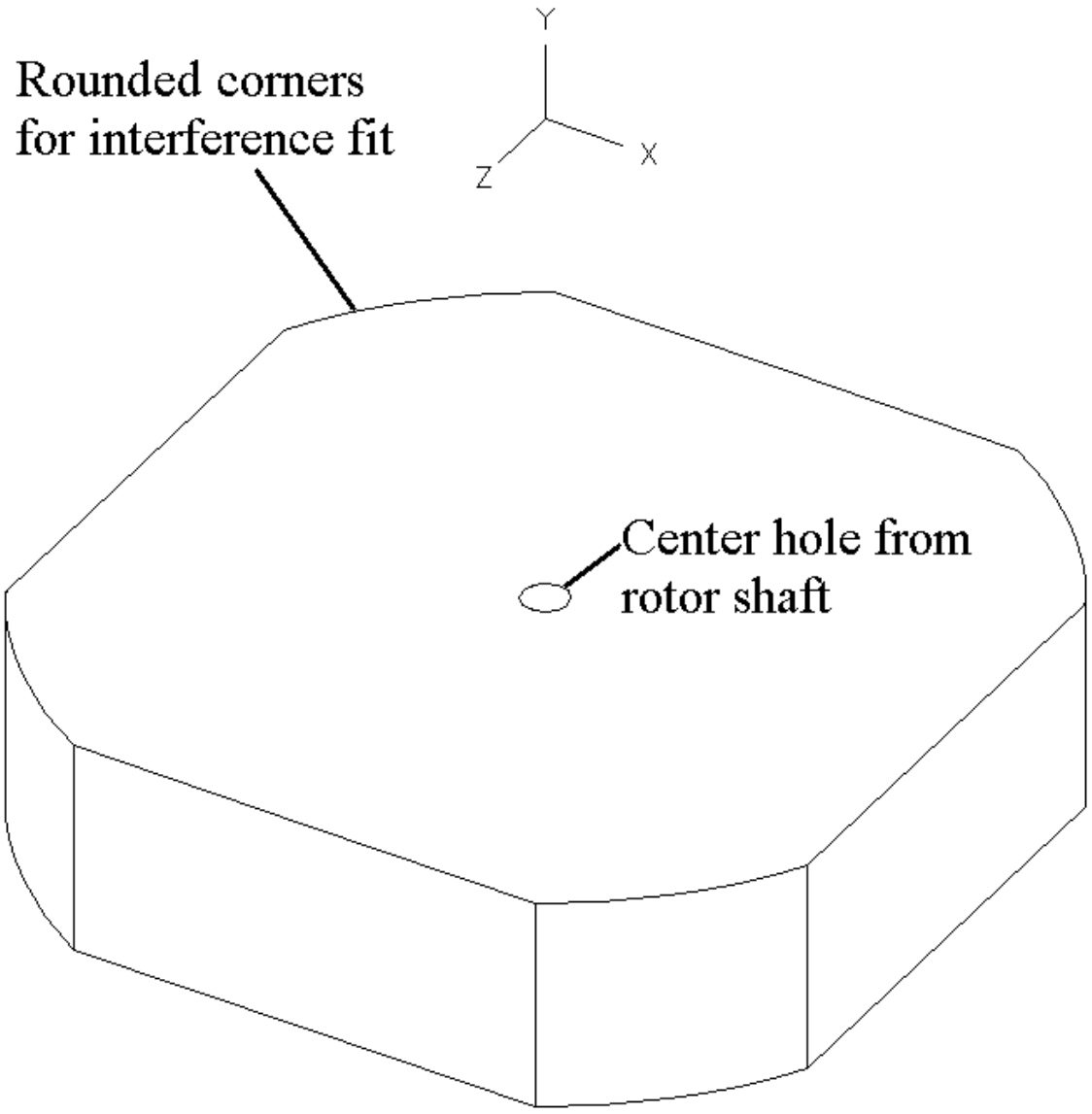

Figure 3. Isometric view of the compression chamber

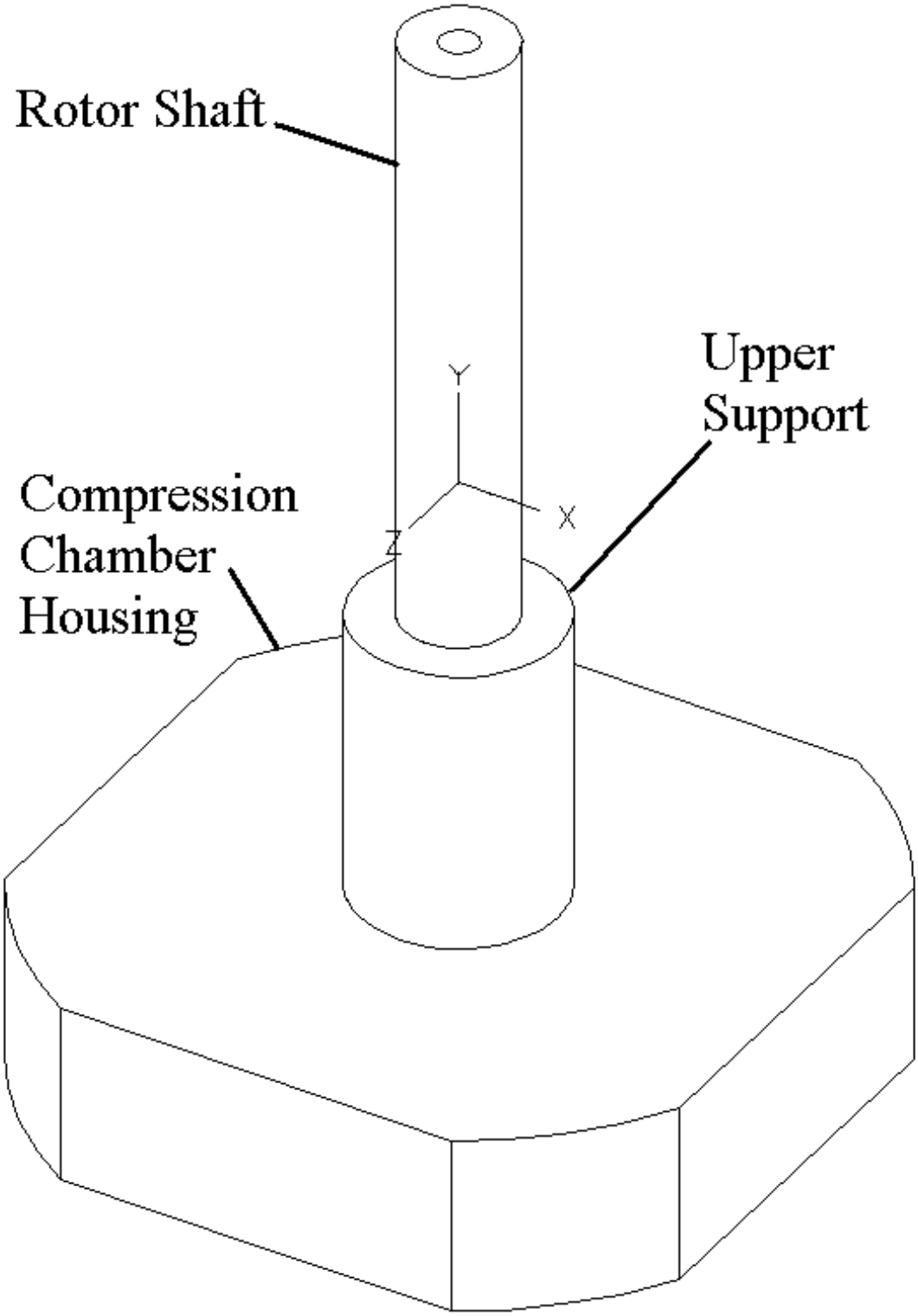

Figure 4. Isometric view of the compression chamber, upper support and rotor shaft

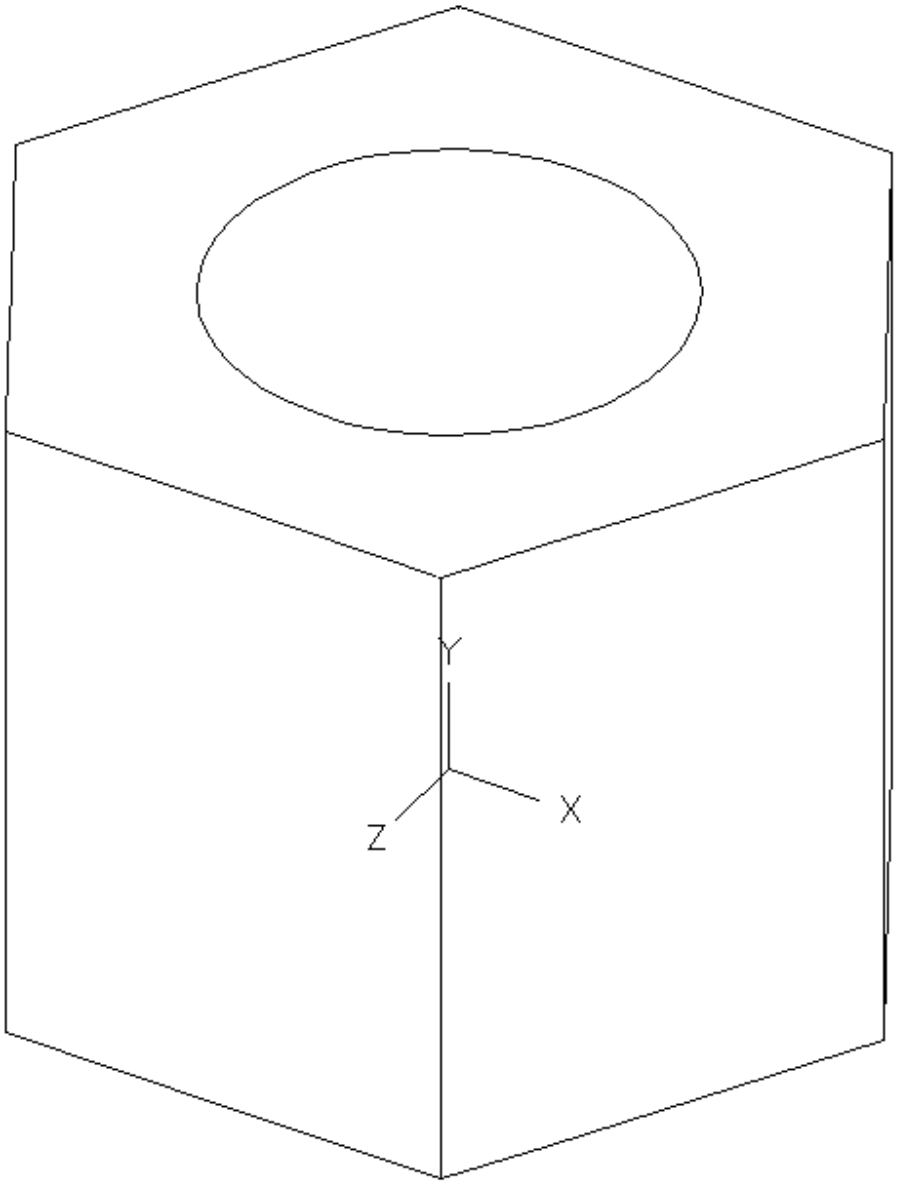

Figure 5. Isometric view of the stator

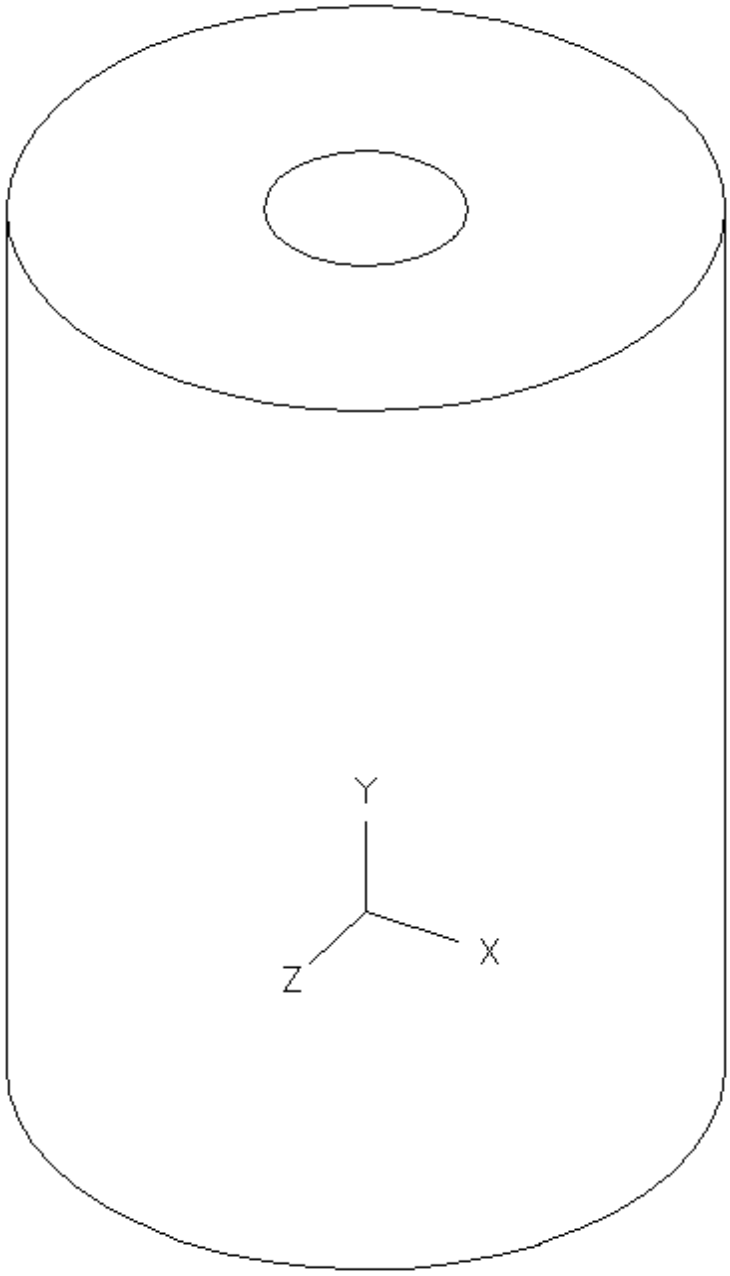

Figure 6. Isometric view of the rotor

The compressor/motor housing was modeled in two sections, upper and lower. The crown and knuckle radii for the ends of such a housing are designed according to the requirements for torispherical flanged and dished heads under internal pressure from the American Society of Mechanical Engineers (ASME) Boiler and Pressure Vessel Code Section VIII, Division 1, Pressure Vessels. The actual equations are available from Chuse [7] and are as follows

$$t = \frac{0.885PL}{SE - 0.1P} \tag{4.2}$$

where

t = minimum thickness, in
P = internal pressure, psi
S = allowable stress, psi
E = minimum joint efficiency, percent
D = inside diameter of head skirt, in
L = inside crown radius, in
r = knuckle radius, in = $0.06L$

However, the only information that was available for constructing the model was a full-scale cross section of the assembly. Therefore, the inside crown radius L for each end was approximated from the full-scale drawing. This was done using the following theorem for the radius of curvature ρ of a line at a point $P(x,y)$ from Swokowski [8]

$$\rho = \frac{|y''|}{\left[1 + (y')^2\right]^{3/2}} \tag{4.3}$$

where the first and second derivatives of y at x are defined using a Newton's central divided difference interpolating polynomial which consists of the following equations:

$$y' = \frac{y_{i+1} - y_{i-1}}{2h} \tag{4.4}$$

$$y'' = \frac{y_{i+1} - 2y_i + y_{i-1}}{h^2} \tag{4.5}$$

where

h = abscissa interval = constant
y_i = i^{th} ordinate value
y' = first derivative of y_i
y'' = second derivative of y_i

Several values for r were calculated for each end of the housing so that a reliable average value for the inside crown radius could be determined. The two knuckle radii were then calculated from the inner crown radii using the above referenced ASME requirement.

The model for the lower section of the compressor housing was simplified in two ways. The first modification was the elimination of the compressor discharge port. The second modification was the deletion of the supports or feet and the stamped plate to which these supports are mounted. The restraints that were applied to the housing during the analyses were applied directly to the outer surface of the lower housing at the midpoint of the contact area between the lower housing and the stamped base plate. See Figure 7 for an isometric view of the lower housing as modeled.

The model for the upper section of the compressor housing was simplified greatly in that all of the bosses and holes were ignored and the piece was assumed to have a constant cross-section revolved around the longitudinal axis, just as the lower section. This approach was taken due to the lack of accurate geometric data available for the upper section and the lack of boundary conditions to be applied to the section. See Figure 8 for an isometric view of the upper housing as modeled.

For review isometric views have been included for the complete rotor/shaft assembly and the complete housing in Figures 9 and 10, respectively. Additionally, a cross-sectional view of the complete compressor assembly as modeled is shown in Figure 11 and an isometric view is shown in Figure 12.

4.4 Finite element selection

All of the compressor/motor components were modeled using three-dimensional eight node linear hexahedron elements. These components included the compressor housing (upper and lower sections), the stator, the rotor, the rotor shaft, the compression chamber housing and the upper support.

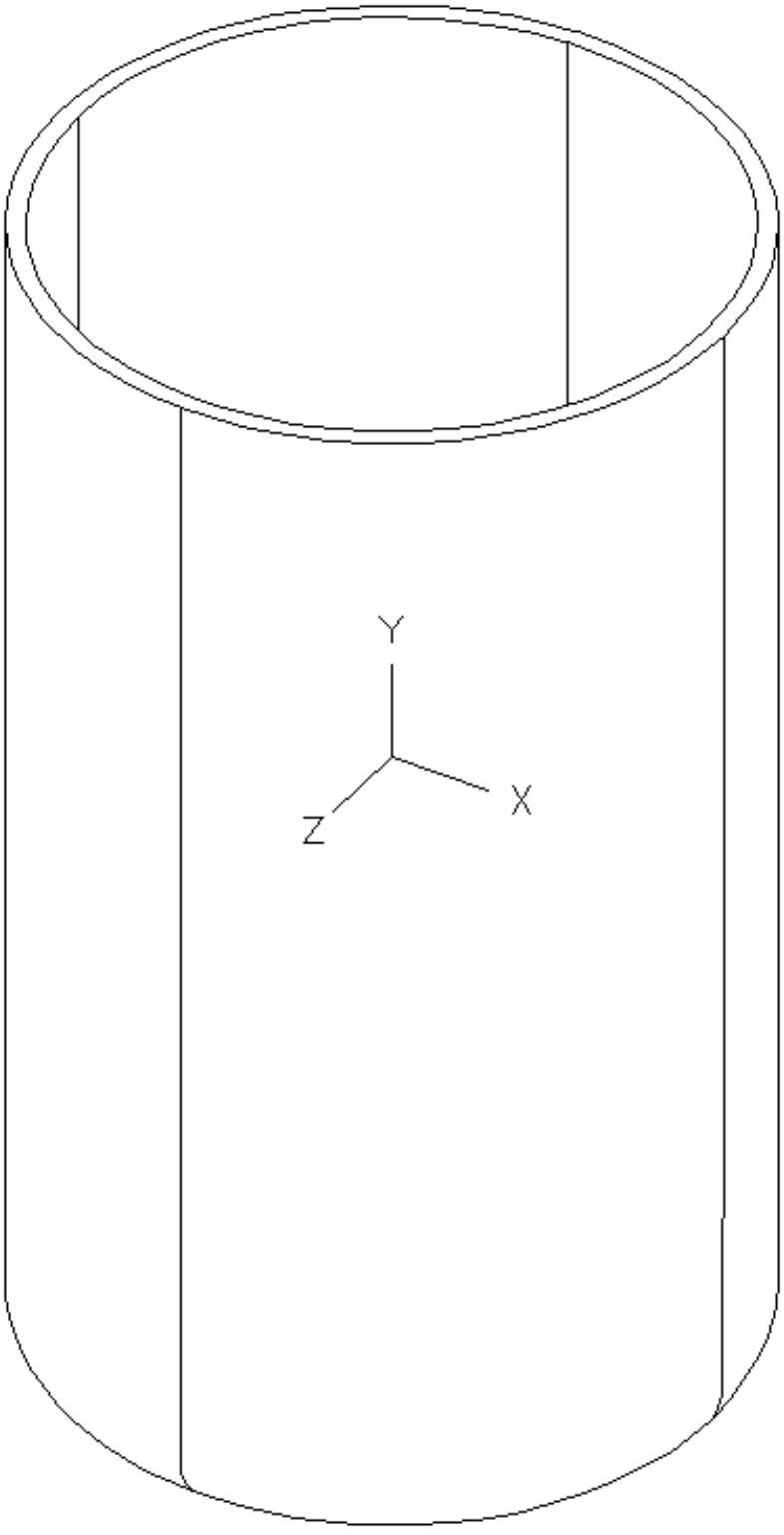

Figure 7. Isometric view of the lower housing

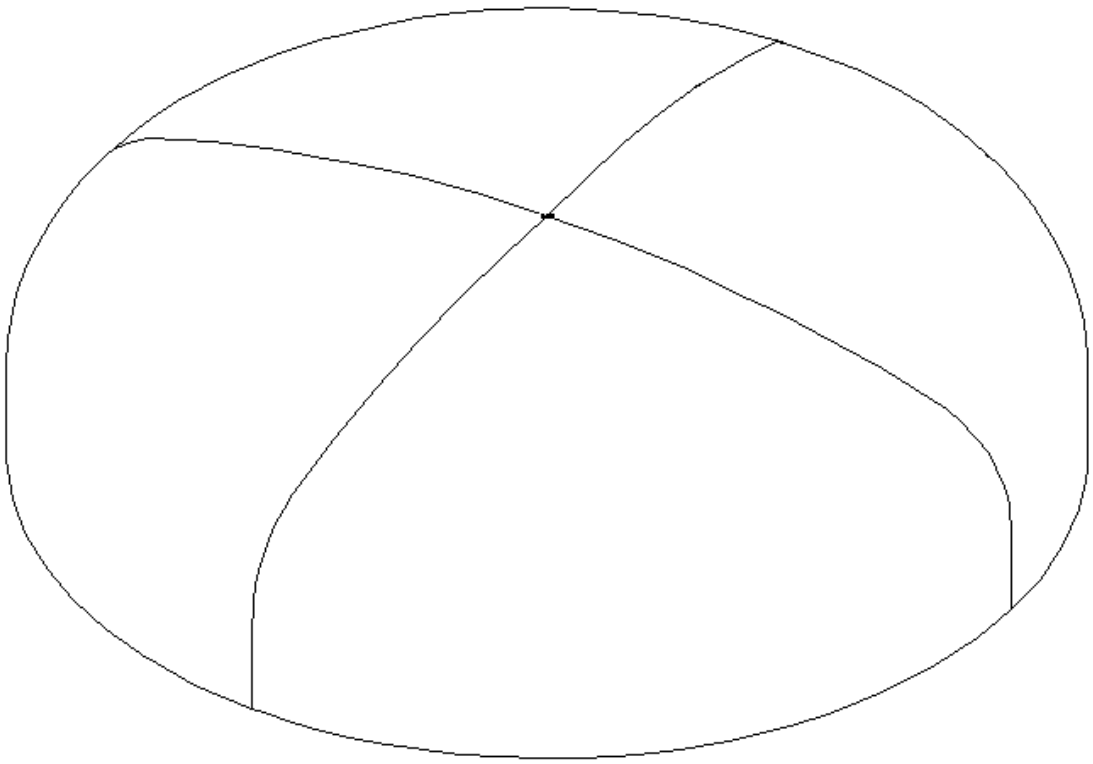

Figure 8. Isometric view of the upper housing

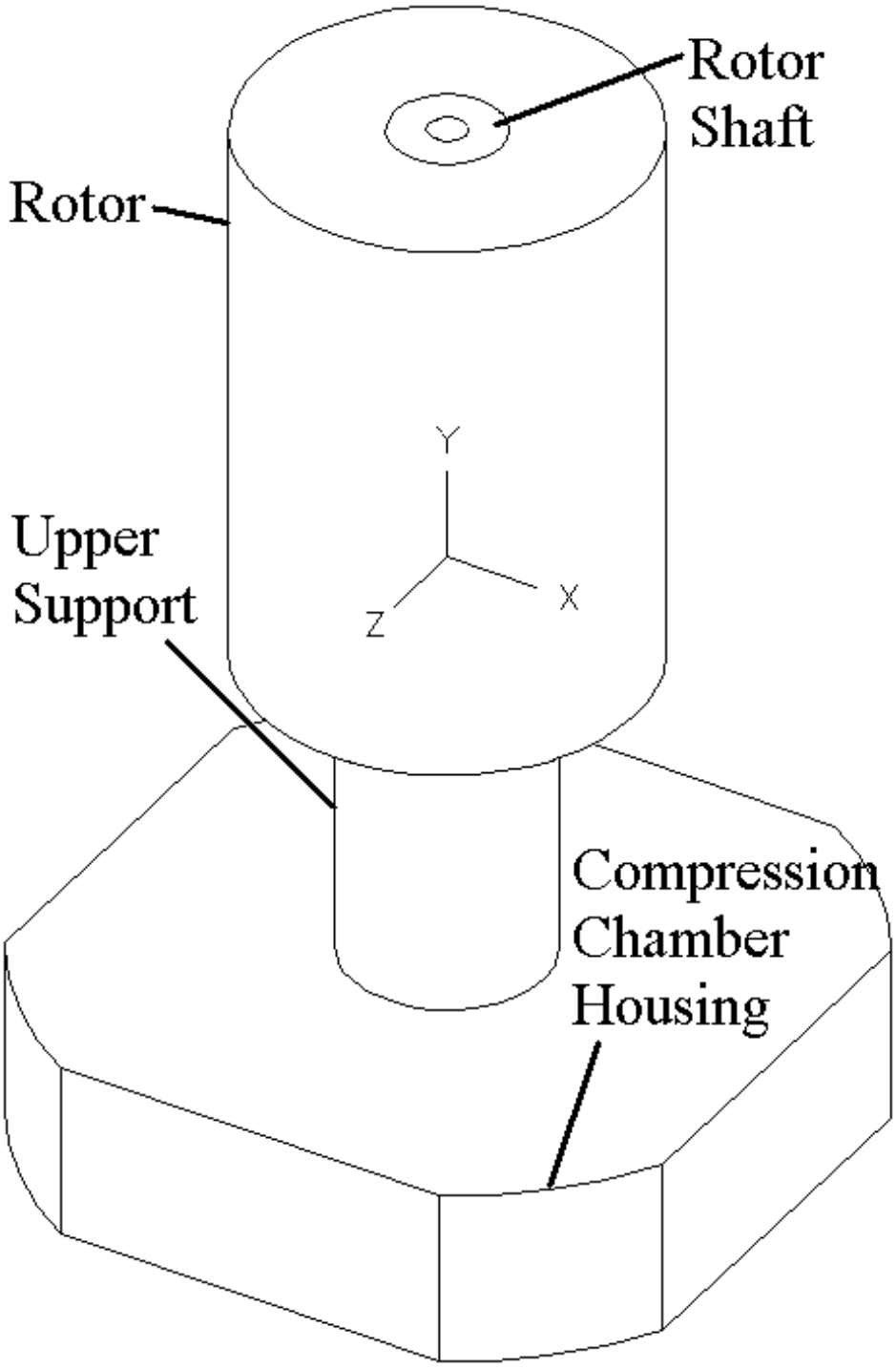

Figure 9. Isometric view of the rotor/shaft assembly

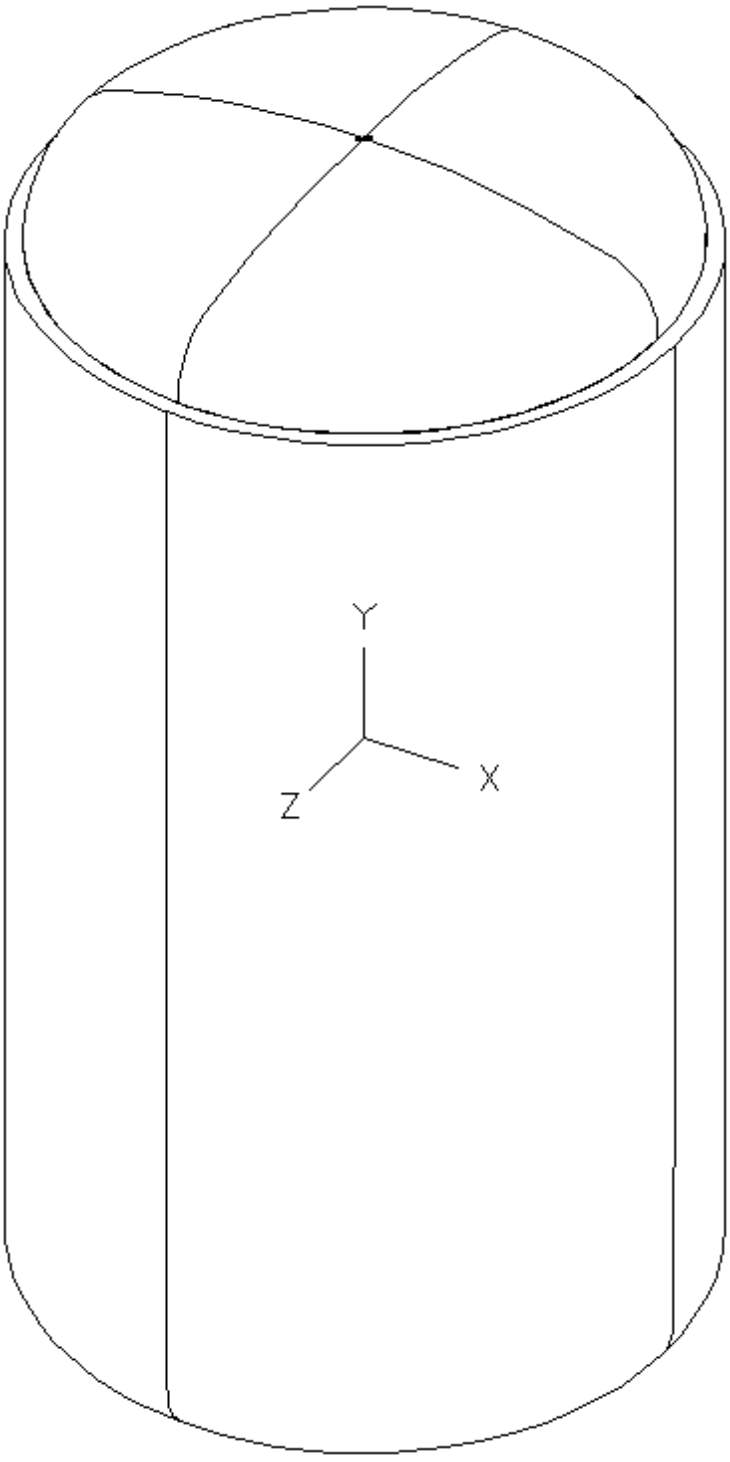

Figure 10. Isometric view of the complete housing

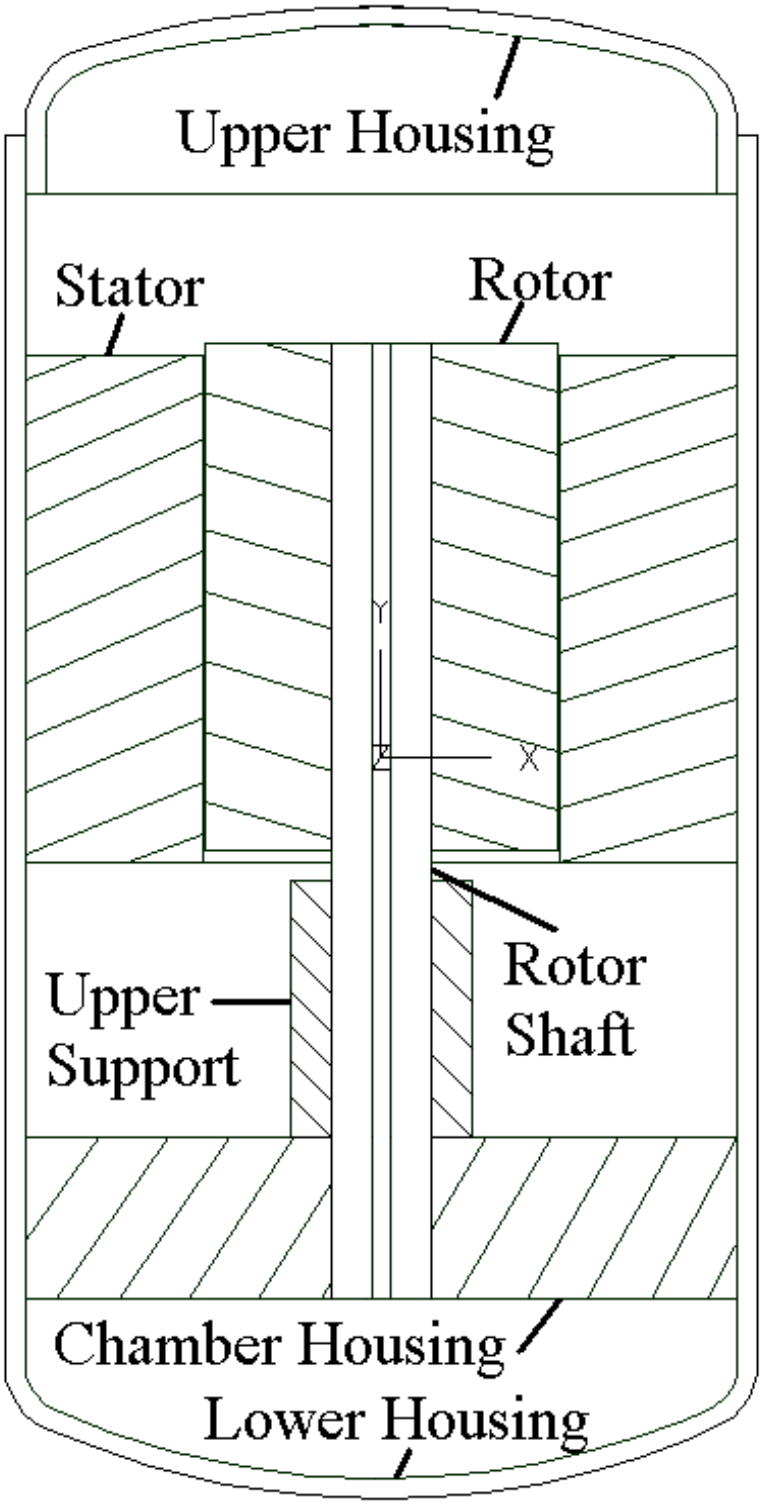

Figure 11. Cross-sectional view of the complete assembly

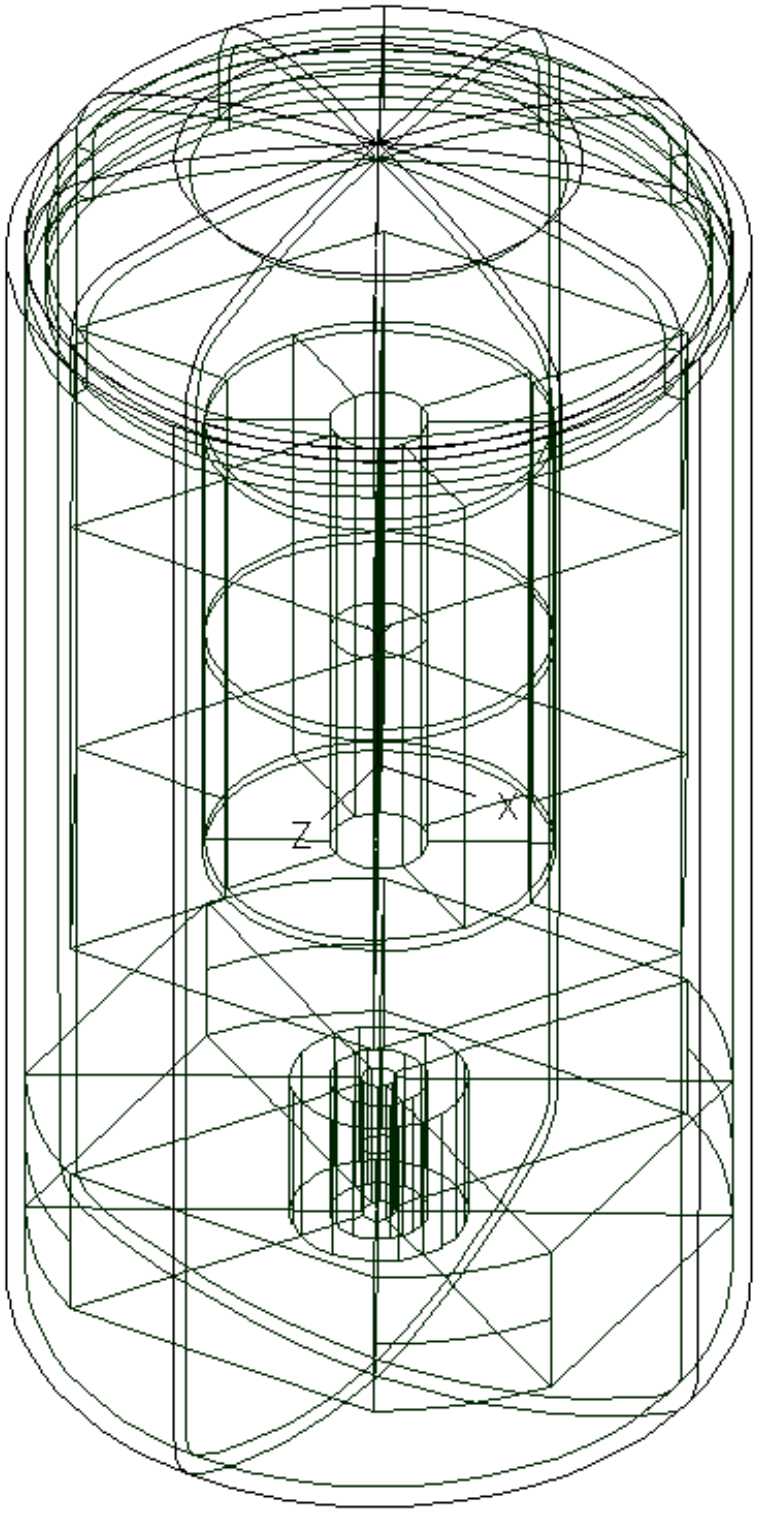

Figure 12. Isometric view of the complete assembly

The need to reassemble the distorted finite element model into parts dictated the use of these three-dimensional solid elements in a mapped mesh on all components except the housing. The housing could have theoretically been modeled more efficiently using thin shell elements. However, the use of shell elements would have required constraint equations to be written between all of the common nodes on the stator, compression chamber housing, and lower housing. Due to the large size of the model and the desire to simplify the modeling process as much as possible, the decision was made to use the same three-dimensional solid elements on the housing as well. While it was recognized that the technique would be less efficient and require more computational run time, it was felt that the total time required for the alternative would be greater. This decision was not made without first checking for accuracy. The complete can was initially modeled by itself using two separate meshes. Each mesh consisted of the same number of elements and featured the same boundary conditions. The first mesh consisted of three-dimensional solid elements while the second mesh consisted of thin shell elements. It was found that the first natural frequency for the two models varied by only 0.52 percent.

The factor of element aspect ratio was also taken into consideration for the decision to use solid elements on the housing. In the I-DEAS software the concept of element aspect ratio is addressed by calculating the relative distortion and stretch factors for the element, where a value of 1.0 is a perfect element and values less than 1.0 are less than perfect. Of the 528 solid elements used to mesh the lower housing the minimum distortion value was 0.80 while the minimum stretch value was 0.30. Of the 264 solid elements used to mesh the upper housing the minimum distortion value was 0.77 while the minimum stretch value was 0.32. It was felt that gross element distortion is the more significant of the two factors. Therefore, the finite element mesh for the housing did not present problems due to abnormal element aspect ratios. Based upon this fact and the small variation in eigenvalue reproduction, the decision to use the three-dimensional solid elements was deemed justifiable. An isometric view of the complete compressor assembly including the finite element mesh is shown in Figure 13.

4.5 Boundary conditions, forcing functions and damping

As stated previously the restraint set used for the analyses of these components consisted of three clamped nodes on the outer surface of the lower housing at 120° radial intervals. This configuration is shown in Figure 14. Each node was at the midpoint of the contact surface between the lower housing and the stamped base plate assembly. These clamped conditions were applied to simulate fastening of the housing base plate to a solid surface by means of threaded fasteners.

The forces applied to the rotor and stator were harmonic inputs at driving frequencies of 29.2 and 120 Hz as described previously. On the outer rotor surface a force of magnitude 0.2 lbf in the positive x-direction was applied to each of the five axial nodes to simulate a unit load. At the corresponding location of the inner stator surface across the air gap, a force of -.0167 lbf in the x-direction was applied to each of the six axial nodes to simulate an equal but opposite unit load.

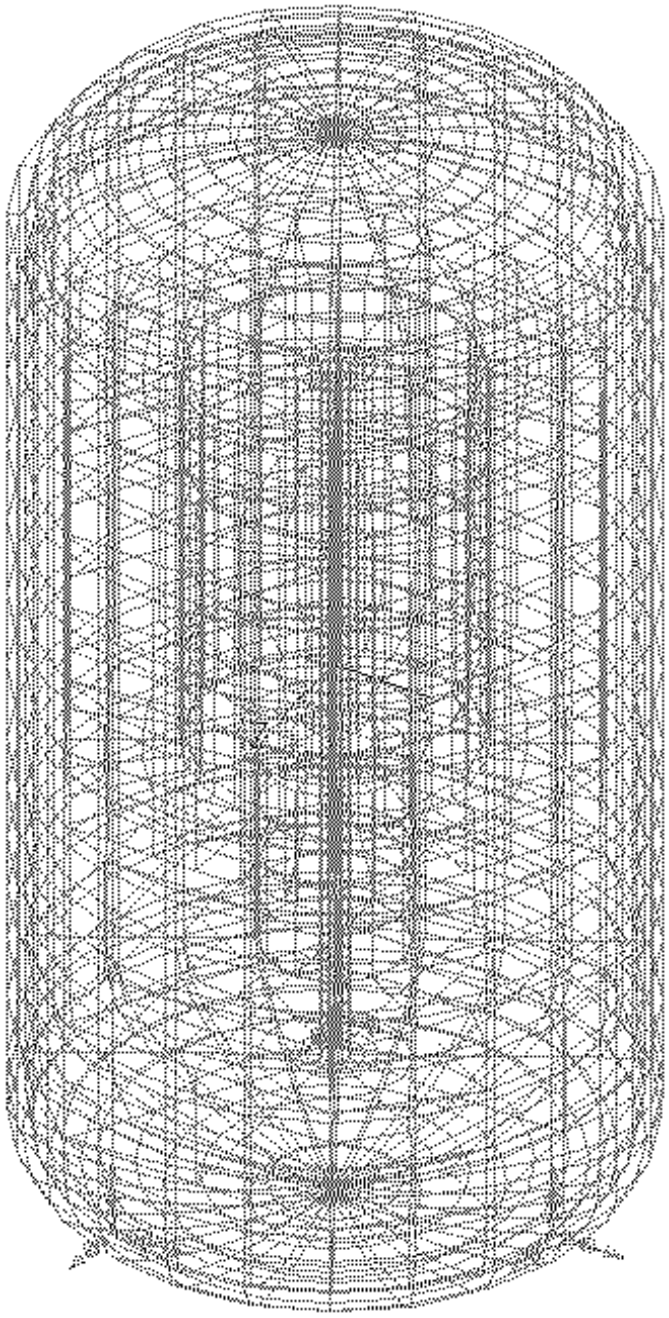

Figure 13. Isometric view of the complete assembly with final finite element mesh

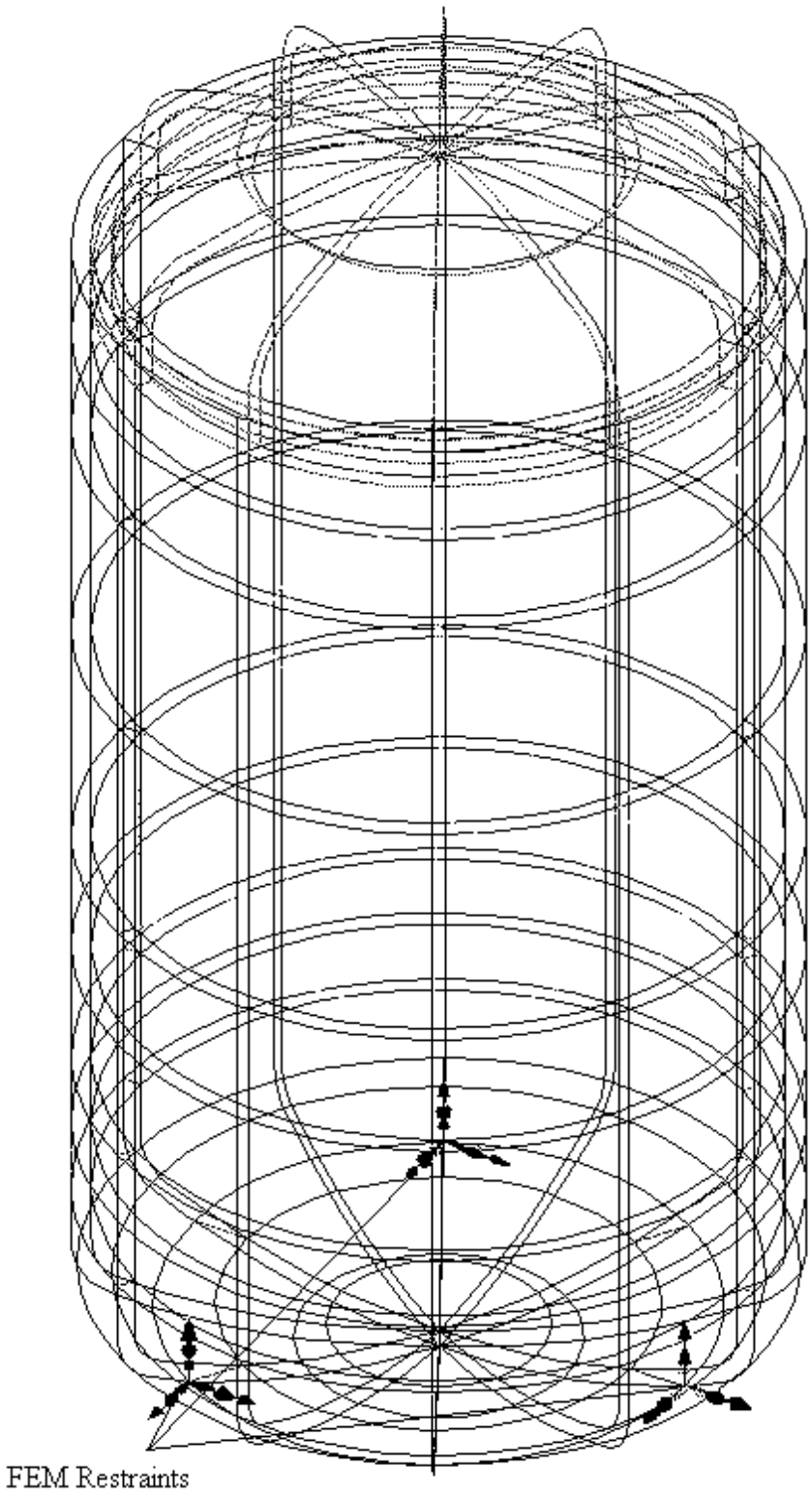

Figure 14. Isometric view of the housing with restraint locations

According to Timar [2] the main source of damping in an electrical machine is the friction on the contact surfaces of the winding and between the core laminations. The amount of damping present is usually derived experimentally with the use of the half-power point method. However, for induction machines, the damping value is normally in the range of 0.01 to 0.04, independent of the mode number. On this basis the amount of damping used for all modes in all finite element models for this research was the average value of this range, 0.025.

4.6 Modeling of joint between upper and lower housing

As stated previously the upper and lower housing sections are assembled by inserting the lower face of the upper housing 1.000 in. into the lower housing and applying a continuous lap weld around the joint perimeter. This method allows the inset portion of the upper housing to remain free to deflect. According to Ramani [9] this type of joint is best modeled by connecting the nodes at the weld by rigid elements and letting the inset nodes of the upper housing remain free. This arrangement appears to best model the joint with respect to resistance of the joint to housing-side motion. In this particular instance the outer diameter of the upper section and the inner diameter of the lower section were modeled as equal. The mapped mesh was dispersed so that a common node between the two sections existed only at the weld joint and not along the inset portion of the upper housing. The use of the *Append* procedure (to be explained in the next section) then allowed the common nodes to become joined through a rigid link. A cross-sectional view of this arrangement is shown in Figure 15.

4.7 Use of the *Append* procedure in assembling the model

As stated the compression chamber and stator both fasten to the lower housing by means of a pressed fit. In many cases this would require that constraint equations be written between the nodes at the chamber/housing and stator/housing interfaces to make the displacements of these nodes equal. Several attempts were made to follow this procedure for the model at hand, but the complexity of the three-dimensional model made this prohibitive. It was discovered that the I-DEAS software contains provisions to link different finite element models into one model. This is known as *appending* models. It is best described by imagining two identical finite element meshes of the same part. However, Mesh 1 has a boundary condition applied at Node 1, while Mesh 2 has a boundary condition applied at Node 2. If these two models are appended the result will be a model that has the appropriate boundary conditions applied at Nodes 1 and 2.

This feature is also very useful for constructing finite element models of components that are joined through a press fit, such as the one under consideration for this analysis. It requires that the mesh of each part is planned so that the coincident nodes of the interfering sections will be at the same location in three-dimensional space. For example, the location of the nodes on the six axial edges of the stator outer surface had to be in the same location as those on six imaginary axial lines of the lower housing inner surface. When mapped meshing and careful planning are utilized in conjunction with this capability the analyst can model and mesh each part individually and then append the separate finite element models into one large model. The *Append* tool proved to be invaluable in this analysis because it also made the task of assigning the different material properties to the respective components much easier.

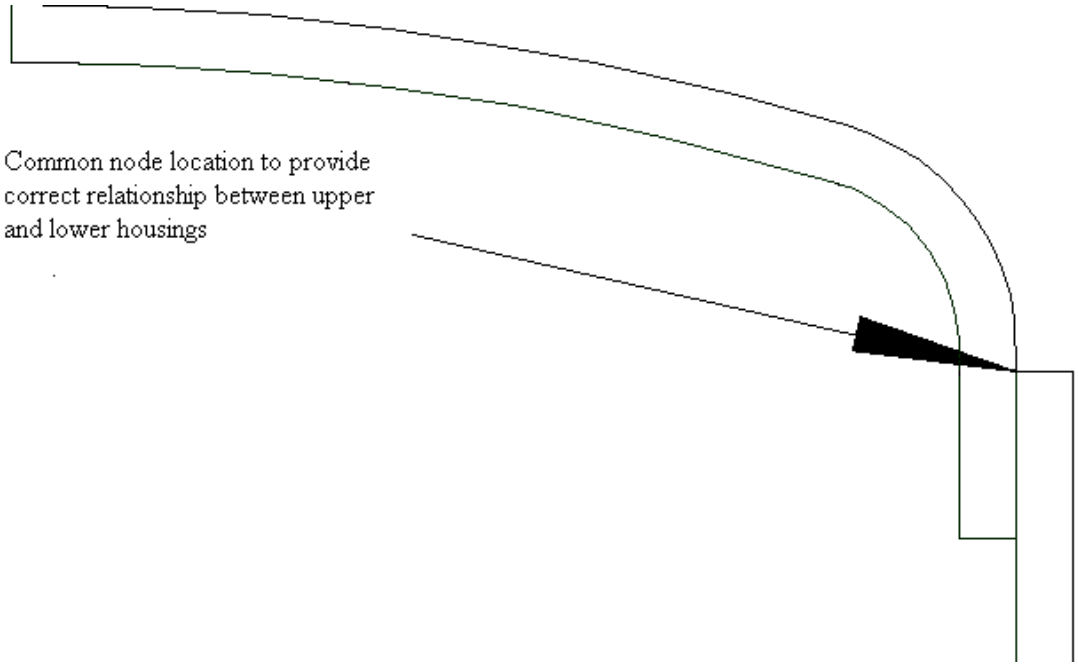

Figure 15. Cross-sectional view of the upper and lower housing interface

Chapter 5.0 Finite element analysis results

5.1 Finite element model verification

While finite element analysis is a powerful tool, its successful application is highly dependent upon the analyst's understanding of the finite element method and the associated pitfalls. Therefore, it is always necessary to validate a finite element model against some other standard. In many cases it is possible to use closed form solutions on simplified geometry for validation. In other cases no form of closed solution may be similar to the actual system. In these instances the only analytical recourse is to perform FEA with different models of the same system to assure that convergence has been reached. The compressor assembly under analysis for this project required both such approaches. After examining all of the components involved it was felt that validation of the rotor/shaft assembly and the housing/stator assembly would be sufficient.

5.1.1 Rotor/shaft assembly model verification

When viewing the cantilever rotor/shaft assembly it can be hypothesized that the compression chamber is analogous to the fixed base of a cantilever beam. Virtually all displacements will occur in the rotor, the upper support collar and the rotor shaft section above the compression chamber. The combined length of the upper support collar and exposed rotor shaft (1.775 in.) is greater than the outside diameters of both the upper support collar (1.110 in.) and the rotor shaft (0.6125 in.). Thus, the assembly may be approximated as a cantilever beam with an additional end mass as shown.

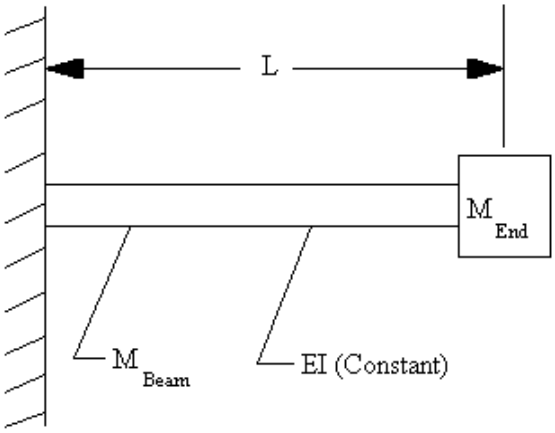

From Rao [6] it is known that this is easily treated as the following single degree of freedom spring-mass system

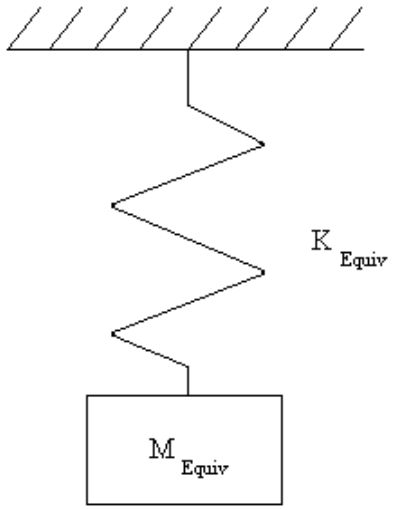

with the following equivalent stiffness K and mass M values.

$$K_{equiv} = \frac{3EI}{L^3} \tag{5.1}$$

$$M_{equiv} = 0.23M_{BEAM} + M_{END} \tag{5.2}$$

where

E = Modulus of Elasticity
I = Area Moment of Inertia
L = length of beam

The problem with this approach is that the section modulus EI for the beam must remain constant. The upper support collar introduces a change in I for the system, thus violating this requirement. The decision was made to analyze the beam using I values for the upper support collar I_1, the rotor shaft I_2 and an equivalent I value weighted for I_1 and I_2.

From Thomson [10] the first natural frequency of a cantilever beam may be found using the following relationship.

$$w_1 = 3.52\sqrt{\frac{EI}{M_{BEAM}L^3}} \tag{5.3}$$

From Cheng [11] it is known that the static deflection of a cantilever beam due to an in-plane force perpendicular to the axial direction as shown may be found through the following relationships.

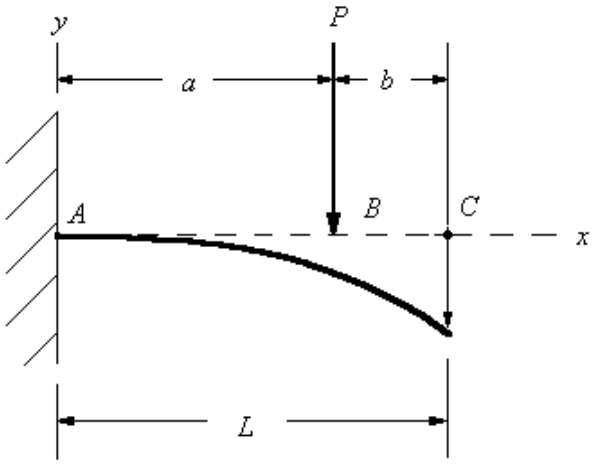

$$y_{AB} = \frac{Px^2}{6EI}(3a - x) \tag{5.4}$$

$$y_{BC} = \frac{Pa^2}{6EI}(3x - a) \tag{5.5}$$

where

y = displacement
P = applied load

Using the three inertia values and an applied load of P = 100 lbf. the first natural frequency ω_1 and the displacement were calculated using the closed form solutions. These results were then compared to those produced by I-DEAS using the final meshing scheme for the assembly on the equivalent geometry. The results are presented in the Table 1.

Table 1. Summary of the mesh verification results for the rotor/shaft assembly

METHOD OF SOLUTION / MOMENT OF INERTIA	FIRST NATURAL FREQUENCY (Hz)	DISPLACEMENT (in.) at $x = L$ DUE TO LOAD APPLICATION AT B
CLOSED FORM / I_1	1444	3.060 E-4
CLOSED FORM / I_2	447	3.339 E-3
CLOSED FORM / I_{EQUIV}	1056	5.860 E-4
I-DEAS / I_{TRUE}	477	4.030 E-4

As can be seen, the first natural frequency for the finite element model is only slightly greater than that found for the cantilever beam with moment of inertia I_2 - a 6.3 percent variation. This variation is due to the greater stiffness K of the finite element model. With respect to displacement, the finite element model is most similar to the cantilever beam with moment of inertia I_1. The model displacement is 24.6 percent greater than the corresponding closed form solution. The smaller deflection exhibited by the closed form solution is due to the larger section modulus EI of the support collar.

5.1.2 Housing/stator assembly model verification

The housing/stator assembly posed significant problems with regards to verifying the finite element model. No closed form solutions exist for any type of thin cylindrical shell with closed ends and a large structural member inside. After careful consideration it was decided that the mesh for this assembly could be verified by ignoring the closed ends of the housing. This decision was based on the following facts.

1) The mesh refinement in these areas was already much greater than that found along the constant cross-section region of the housing. This aspect was a byproduct of the need to partition the housing into sections to apply the mapped mesh.
2) The true shape of the upper housing was not known and therefore, could not be modeled accurately.
3) The lack of boundary conditions in association with the upper housing.
4) The contribution to the total housing stiffness by the stator and the compression chamber, which are located in the region of constant cross-section.

5) The short axial distance between the constrained nodes on the lower housing end and the lower face of the compression chamber.

Thus to validate the mesh applied to the stator and housing for the analysis of the complete unit, the housing was treated as a cantilevered cylinder. The length of this cylinder was equal to the axial distance from the bottom face of the compression chamber to the top face of the stator. The stator was included, and its upper face was set flush with the free end of the housing. A cross-sectional view of this assembly with the restraint and load locations is shown in Figure 16.

It was initially thought that the stator and housing model could also be treated as a cantilever beam with an additional end mass. Therefore, displacements and natural frequencies were calculated using both finite element analysis and the closed form solutions. Upon comparison of the results it was realized that this approach was not feasible. The 4.625 in. outer housing diameter is greater than the 4.275 in. equivalent beam length. Therefore, all assumptions made by conventional beam theory are invalid. The only possible non-numerical solution approach to this problem would be the use of the theory of elasticity.

After deliberation, the decision was made to analyze the assembly with several different finite element meshes to assure convergence. As stated previously the use of the *Append* procedure and mapped meshing required that all of the components be partitioned into several sections. The housing was partitioned axially and circumferentially, while the stator was partitioned only circumferentially. The partitions of the open housing and the stator are shown in Figures 17 and 18, respectively. Because varying the housing mesh density in the radial direction would introduce extreme element distortion, it was decided to vary the mesh density along the different axial and circumferential partitions. Using the actual mesh densities from the complete compressor model as a baseline, the density in each region was increased by a substantial margin. For each of these mesh densities the first several natural frequencies and the displacements due to a 100 lbf. radial load applied at the free end would be calculated and compared to assure convergence. A top view of the housing/stator assembly and the applied force is shown in Figure 19.

The housing as tested was partitioned axially into three sections – lower, middle and upper (see Figure 17). The lower section length was equal to the compression chamber thickness, the upper section length was equal to the stator length and the middle section length was equal to the axial distance between the compression chamber and stator. The baseline element distribution in the axial direction was

1) lower section – two elements
2) middle section – four elements and
3) upper section – five elements.

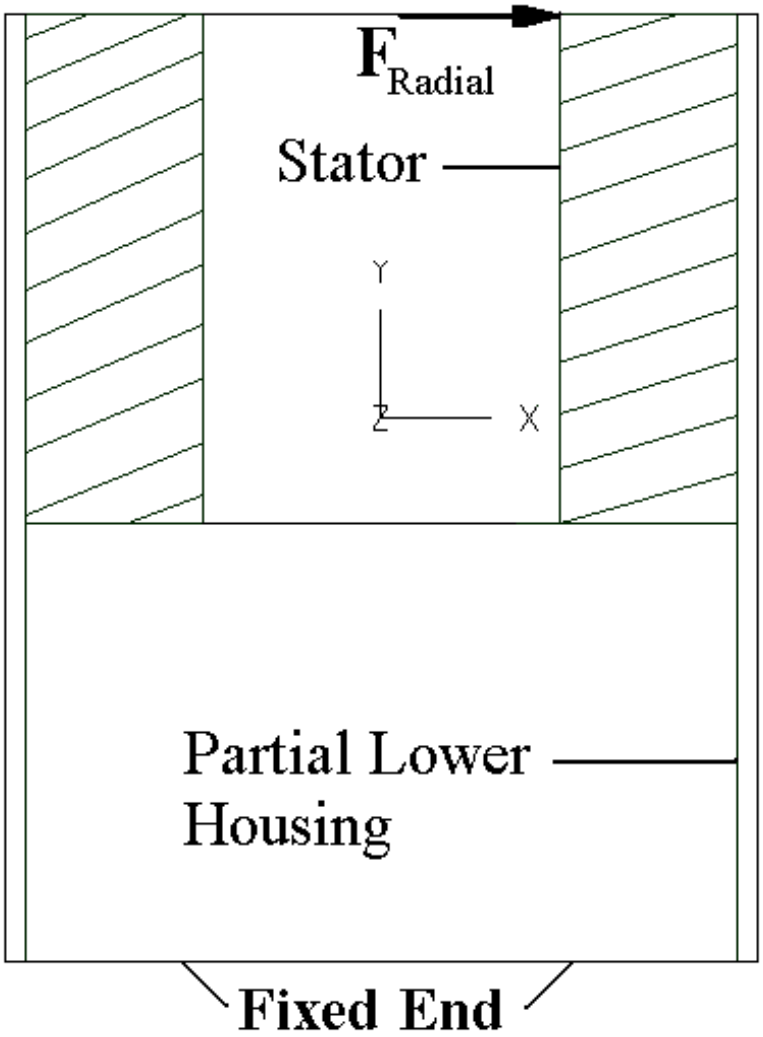

Figure 16. Cross-sectional view of the partial lower housing and stator

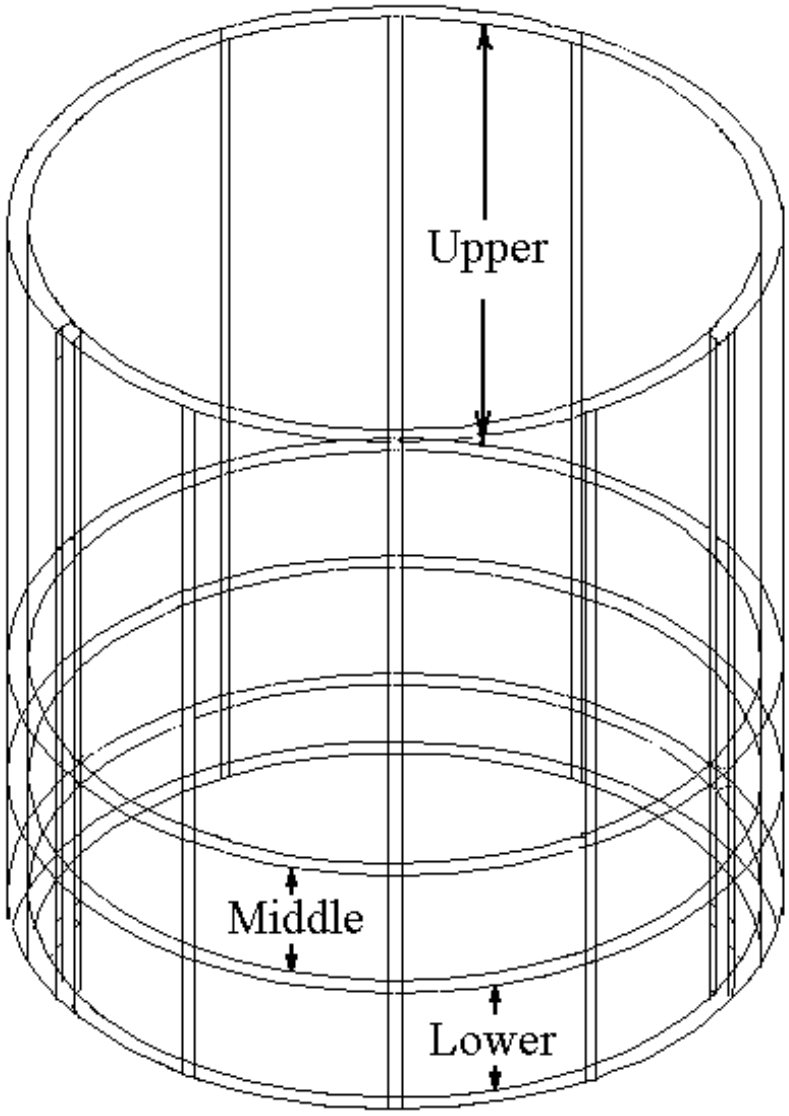

Figure 17. Isometric view of the partitioned partial lower housing

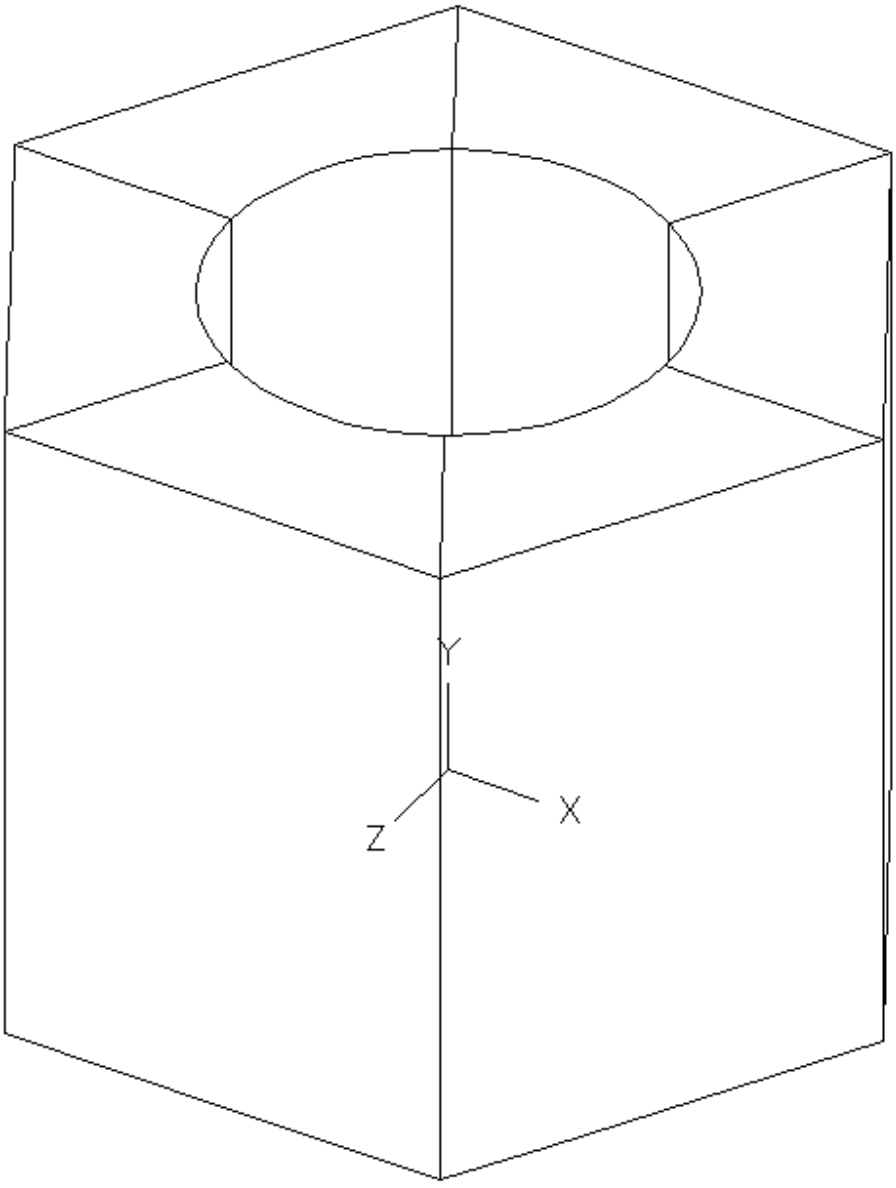

Figure 18. Isometric view of partitioned stator

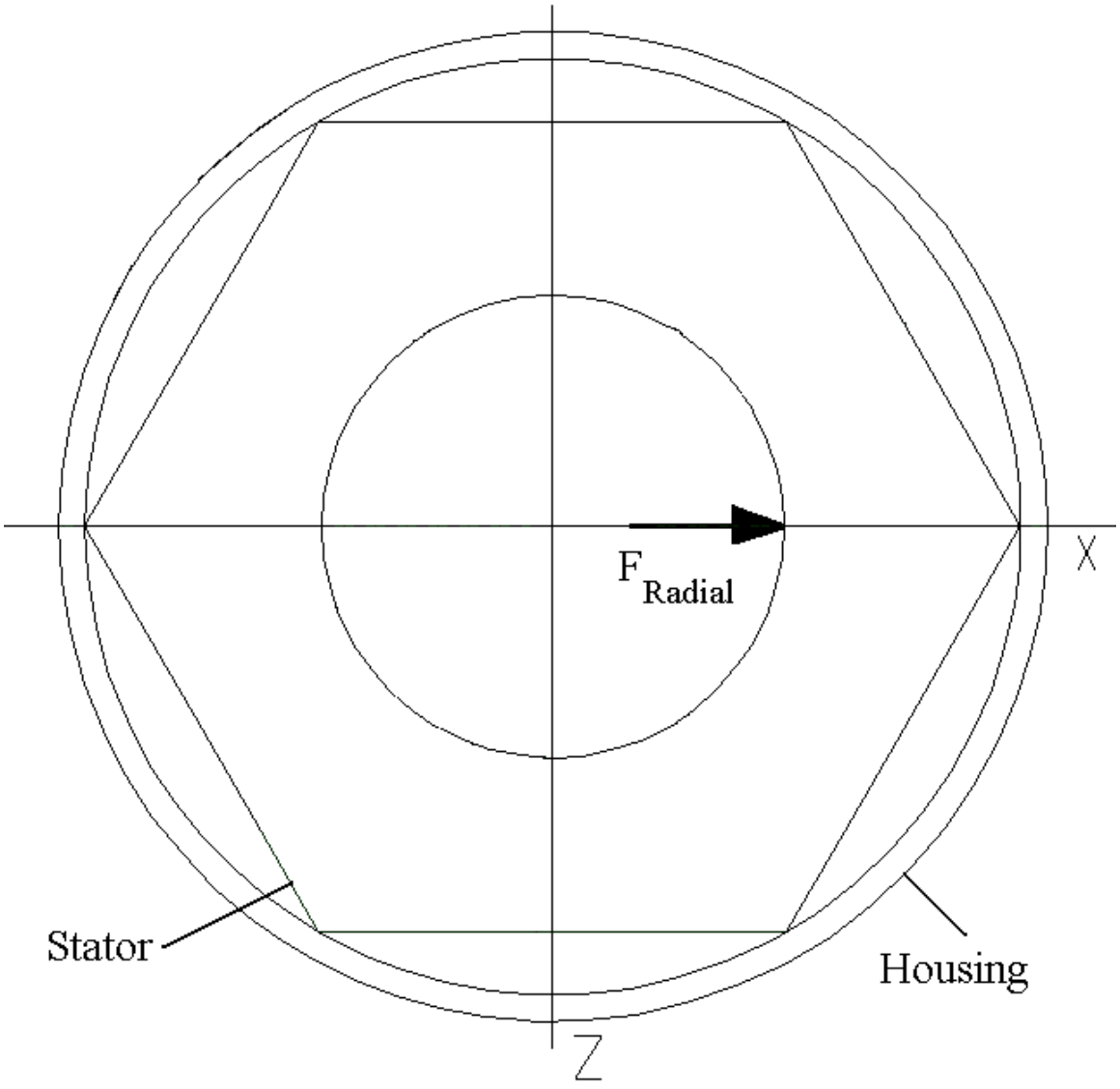

Figure 19. Cross-sectional view of the partial housing/stator assembly with the applied force

The housing and stator were each partitioned circumferentially into six sections. The baseline element distribution in the circumferential direction for the housing was four elements per section. The optimal circumferential element distribution for the stator was determined in separate tests to be six elements per section. This partitioning scheme provided the common axial locations required to append the housing and stator together into a single finite element model.

The mesh variations and the resulting natural frequencies and displacements are shown in Table 2.

Table 2. Summary of the mesh verification results for the partial housing/stator assembly

MESH DENSITY	ω_1 (Hz)	ω_2 (Hz)	ω_3 (Hz)	Y_{max} (in.)	$\Delta\omega_1$ (%)	ΔY_{max} (%)
Original	1366.45	1366.45	3081.08	7.90 E-05	0.00	0.00
Lower axial +50%	1364.83	1364.84	3081.33	7.93 E-05	0.12	-0.28
Lower axial +100%	1364.05	1364.05	3081.41	7.94 E-05	0.18	-0.42
Middle axial +25%	1365.88	1365.88	3079.59	7.91 E-05	0.04	-0.08
Middle axial +50%	1365.52	1365.52	3078.62	7.91 E-05	0.07	-0.11
Upper axial +20%	1365.83	1365.83	3077.33	7.91 E-05	0.05	-0.08
Upper axial +40%	1365.38	1365.38	3074.78	7.91 E-05	0.08	-0.14
Circumferential +50%	1360.08	1360.08	3055.62	7.95 E-05	0.47	-0.57
Circumferential +100%	1357.83	1357.83	3048.21	7.96 E-05	0.63	-0.75

As can be seen all differences in the displacement and first natural frequency are less than one percent. Based upon these results it was decided that the mesh density used in the complete assembly had reached convergence and was fully acceptable.

5.2 Eigenvalue results

After validation of the finite element model the next step was to determine the lower eigenvalues of the various components. The need to calculate these eigenvalues was twofold. The first reason was to determine if the operating frequency of the rotor was close to one of the lower natural frequencies of the system. The second reason was that the ultimate goal of this project was to determine the system response to the harmonic force inputs. Since the I-DEAS software

uses modal superposition as described in Chapter 4 to solve for cases of systems subjected to the input of dynamic forces, the solution of the eigenvalue value problem was required.

Eigenvalue analyses were performed on the following combinations of components:

1) the rotor/shaft assembly consisting of the compression chamber housing, rotor shaft, upper support and rotor
2) the housing/stator assembly consisting of the upper and lower housings and the stator
3) the entire compressor assembly

The first five eigenvalues calculated using the I-DEAS software for these three combinations are listed in Table 3.

Table 3. Eigenvalue results for the various system components

	Rotor/Shaft Assembly	**Housing/Stator Assembly**	**Complete Compressor Assembly**
Eigenvalue #1 (Hz)	324.23	290.90	240.37
Eigenvalue #2 (Hz)	337.85	290.91	242.64
Eigenvalue #3 (Hz)	1030.12	1252.88	373.61
Eigenvalue #4 (Hz)	2300.33	1838.16	388.98
Eigenvalue #5 (Hz)	2444.10	3131.29	991.28

As is evident from Table 3 none of the major component assemblies has an eigenvalue close to the 29.2 Hz operating frequency of the machine. Nor do any of the assemblies have an eigenvalue close to the twice voltage supply frequency of 120 Hz. The first eigenvalue of the complete compressor assembly occurs at 240 Hz. It can be noted that this value is equivalent to approximately the eighth harmonic of the rotational frequency and the second harmonic of the twice voltage supply frequency.

5.3 Displacements due to harmonic force inputs

As described previously the purpose of the finite element analysis for this project was to determine the displacement of the system when subjected to harmonic force inputs characteristic of unbalanced magnetic pull. The location, magnitude, and frequency of these functions were described in Chapter 4.

It was described in Chapters 3 and 4 that the ability to reproduce the stator/rotor interference for visual inspection using geometric entities was highly desirable. While much time and effort were put into creating these reproductions, it was found upon analysis of the actual compressor model that the technique developed was inadequate. The developed procedure was highly dependent upon the analyst's ability to zoom in to small areas of the displaced finite element model and pick various points. Upon application to the final compressor mesh it was found that this ability did

not exist. At that time it became apparent that two erroneous assumptions were made during the development of this procedure.

1) It was assumed that the mesh of the compressor model could be made relatively coarse and still maintain accuracy.
2) It was assumed that each displaced component (i.e., the displaced rotor and the displaced stator) could be analyzed individually, thus providing clear access to all of the nodes. This assumption was made before it was known that the meshes of the independent components would have to be appended into a final model.

Upon performing the analyses on the final compressor model it was found that the required mesh density, along with the inability to remove unnecessary objects from the screen, made picking individual points on a specific surface virtually impossible.

At this point it was decided to examine specific nodes on the outer rotor surface and inner stator surface with respect to displacement. These nodes were located at 0, 90, 180 and 270 degrees when viewing the compressor assembly from the top just below the upper housing, as seen in Figure 20. The harmonic force inputs to the system were applied at the 0-degree location perpendicular to the shaft axis as shown in Figure 21. The nodes at these locations were examined along the entire length of the rotor and stator surfaces. While this procedure did require the task of determining the individual node labels, it proved to be a much more reasonable approach than picking nodes for surface reproduction. This was because the node labels could be determined before the meshes were displaced. Once the node labels were known the analyses could be run and the resulting displacements could be examined in column form through the I-DEAS post-processing capabilities.

As stated there were five nodes dispersed along the axial direction of the rotor and six nodes along the axial direction of the stator. Since the displacements were examined at the four points in the plane perpendicular to the axial direction, twenty and twenty-four points were examined on the rotor and stator surfaces, respectively, for each applied harmonic force. The six stator displacements along each axial line were then interpolated to give displacements at five points, thus providing a 1:1 ratio with the rotor surface displacements. A simple schematic depicting this transition is shown in Figure 22. These global displacements will be listed in tabular form and graphical form in the following sections. Rather than use the actual node numbers assigned by I-DEAS the nodes will be labeled 1-5 with 1 being at the top or free end of the stator and rotor and 5 being at the bottom end. For these analyses the compressor assembly was located in three-dimensional space so that the applied forces occur in the X-direction of the XY-plane. Thus all Z-displacements are perpendicular and out of plane to the applied force.

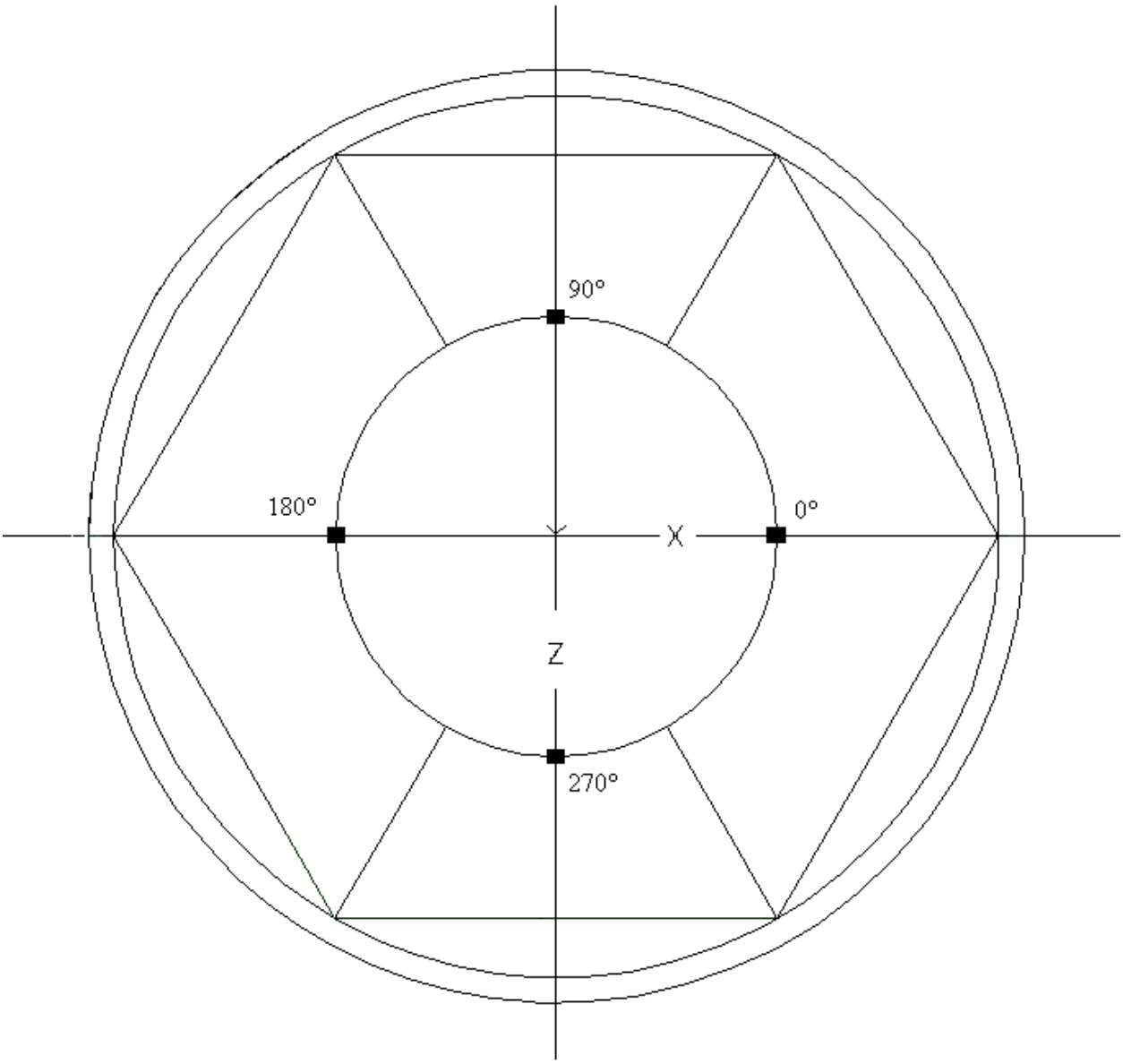

Figure 20. Locations of the 0°, 90°, 180° and 270° points on the motor assembly

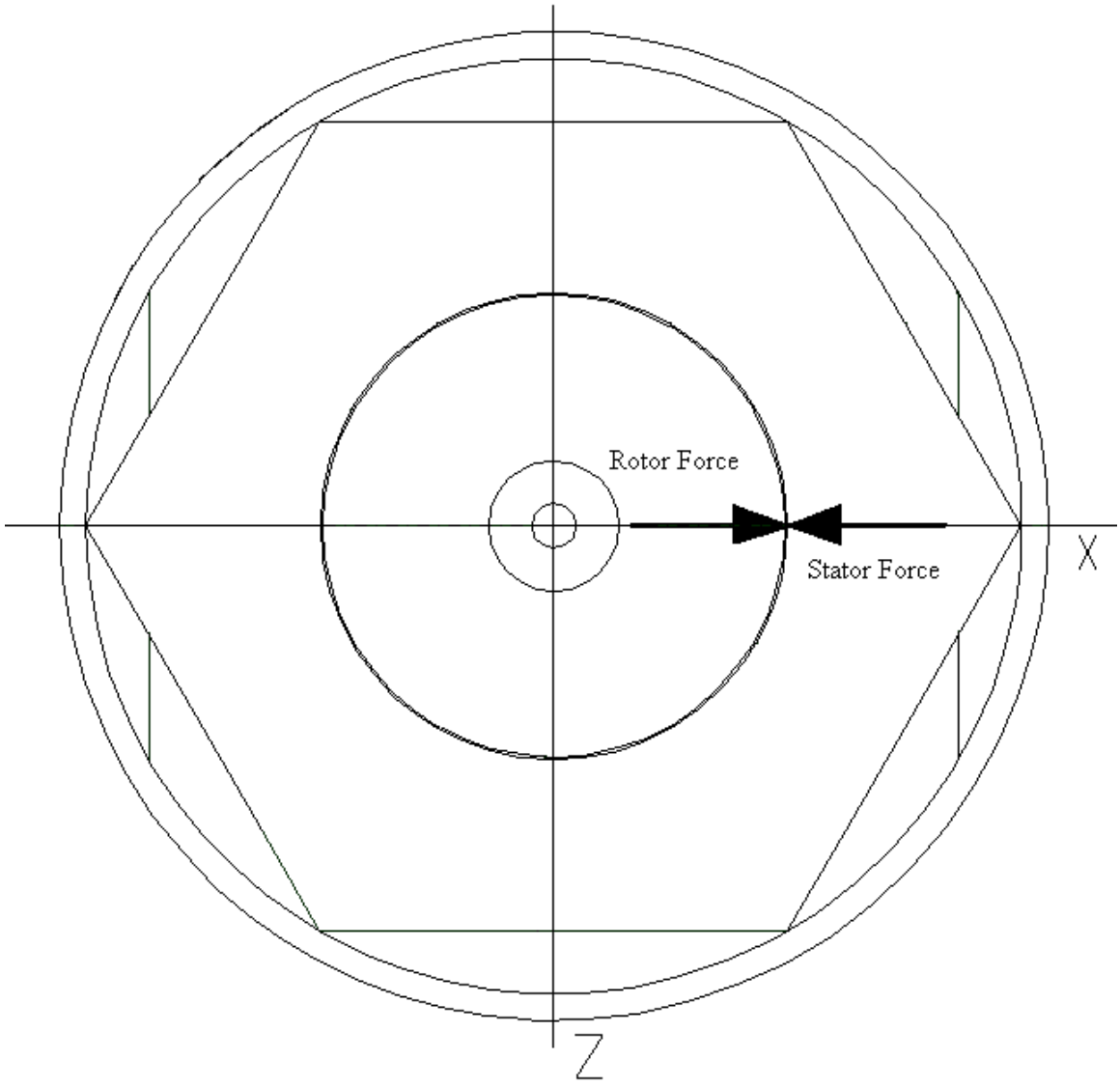

Figure 21. Orientation of the stator and rotor harmonic force inputs

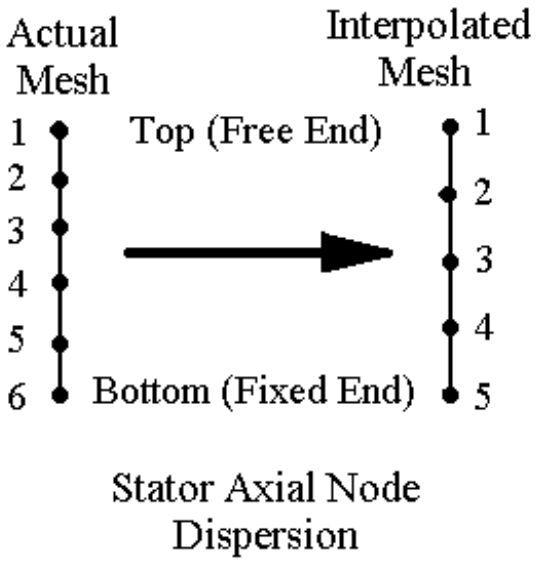

Figure 22. Depiction of stator nodal information interpolation

5.3.1 Displacements due to 29.2 Hz input

The rotor and stator displacements due to the 29.2 Hz harmonic force inputs on the rotor and stator are listed in Tables 4-11 and Figures 23-28 for the 0, 180, 90 and 270 degree locations.

Table 4: Rotor displacement at 0° due to 29.2 Hz force input on stator and rotor

NODE NUMBER	X DISPLACE. (in.)	Y DISPLACE. (in.)	Z DISPLACE. (in.)
1	4.435 E-05	-1.273 E-05	1.533 E-09
2	3.508 E-05	-1.273 E-05	1.491 E-09
3	2.581 E-05	-1.271 E-05	1.442 E-09
4	1.655 E-05	-1.270 E-05	1.392 E-09
5	7.245 E-06	-1.270 E-05	1.346 E-09

Table 5: Rotor displacement at 180° due to 29.2 Hz force input on stator and rotor

NODE NUMBER	X_DISPLACE. (in.)	Y_DISPLACE. (in.)	Z_DISPLACE. (in.)
1	4.435 E-05	1.273 E-05	-9.938 E-10
2	3.508 E-05	1.273 E-05	-1.034 E-09
3	2.581 E-05	1.271 E-05	-1.075 E-09
4	1.655 E-05	1.271 E-05	-1.116 E-09
5	7.245 E-06	1.270 E-05	-1.132 E-09

Table 6: Rotor displacement at 90° due to 29.2 Hz force input on stator and rotor

NODE NUMBER	X_DISPLACE. (in.)	Y_DISPLACE. (in.)	Z_DISPLACE. (in.)
1	4.435 E-05	4.904 E-07	2.961 E-10
2	3.508 E-05	4.903 E-07	2.016 E-10
3	2.580 E-05	4.896 E-07	5.367 E-10
4	1.653 E-05	4.894 E-07	1.174 E-09
5	7.282 E-06	4.897 E-07	-9.834 E-10

Table 7: Rotor displacement at 270° due to 29.2 Hz force input on stator and rotor

NODE NUMBER	X_DISPLACE. (in.)	Y_DISPLACE. (in.)	Z_DISPLACE. (in.)
1	4.435 E-05	4.899 E-07	1.477 E-10
2	3.508 E-05	4.897 E-07	1.590 E-10
3	2.580 E-05	4.890 E-07	-2.586 E-10
4	1.653 E-05	4.888 E-07	-9.775 E-10
5	7.280 E-06	4.891 E-07	1.092 E-09

Table 8: Stator displacement at 0° due to 29.2 Hz force input on stator and rotor

NODE NUMBER	X_DISPLACE. (in.)	Y_DISPLACE. (in.)	Z_DISPLACE. (in.)
1	-1.748 E-07	3.835 E-08	1.010 E-11
2	-1.445 E-07	3.812 E-08	9.522 E-12
3	-1.148 E-07	3.844 E-08	8.933 E-12
4	-8.795 E-08	3.934 E-08	8.367 E-12
5	-6.508 E-08	3.942 E-08	7.803 E-12

Table 9: Stator displacement at 180° due to 29.2 Hz force input on stator and rotor

NODE NUMBER	X DISPLACE. (in.)	Y DISPLACE. (in.)	Z DISPLACE. (in.)
1	-1.746 E-07	-3.631 E-08	-7.024 E-12
2	-1.444 E-07	-3.605 E-08	-7.579 E-12
3	-1.148 E-07	-3.638 E-08	-8.121 E-12
4	-8.800 E-08	-3.729 E-08	-8.648 E-12
5	-6.529 E-08	-3.738 E-08	-9.167 E-12

Table 10: Stator displacement at 90° due to 29.2 Hz force input on stator and rotor

NODE NUMBER	X DISPLACE. (in.)	Y DISPLACE. (in.)	Z DISPLACE. (in.)
1	-1.729 E-07	1.008 E-09	-6.949 E-11
2	-1.439 E-07	1.002 E-09	-4.363 E-11
3	-1.139 E-07	1.002 E-09	-1.024 E-11
4	-8.559 E-08	1.007 E-09	3.905 E-11
5	-5.995 E-08	1.014 E-09	1.064 E-10

Table 11: Stator displacement at 270° due to 29.2 Hz force input on stator and rotor

NODE NUMBER	X DISPLACE. (in.)	Y DISPLACE. (in.)	Z DISPLACE. (in.)
1	-1.729 E-07	1.007 E-09	7.257 E-11
2	-1.439 E-07	1.000 E-09	4.560 E-11
3	-1.139 E-07	1.000 E-09	1.089 E-11
4	-8.561 E-08	1.005 E-09	-3.914 E-11
5	-5.997 E-08	1.012 E-09	-1.072 E-10

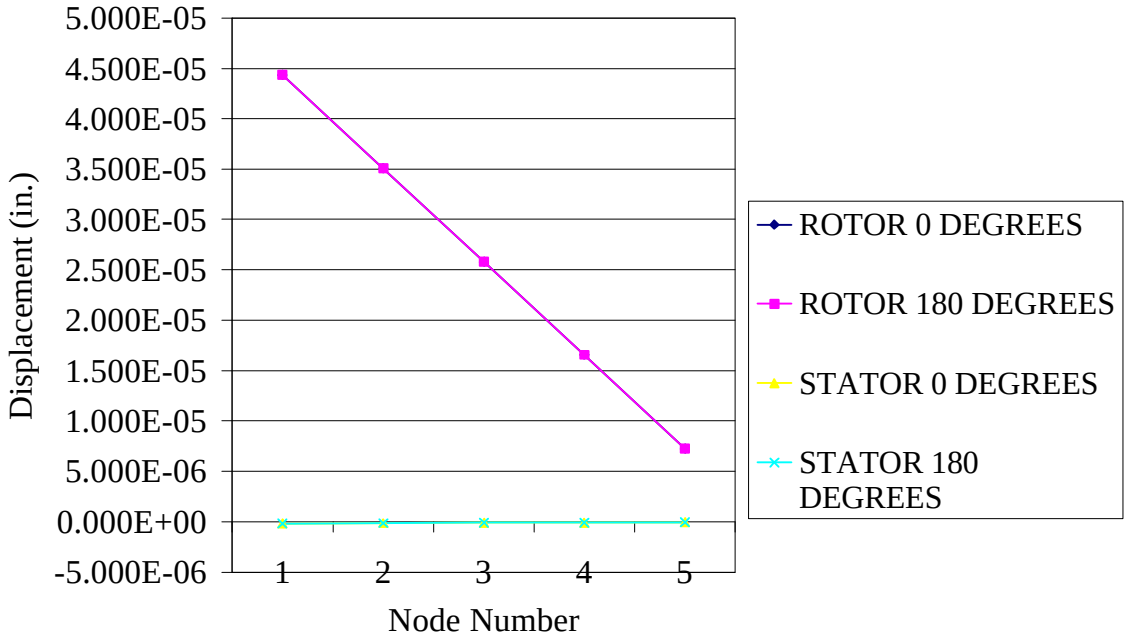

Figure 23. Rotor and Stator X-axis displacements due to 29.2 Hz force input

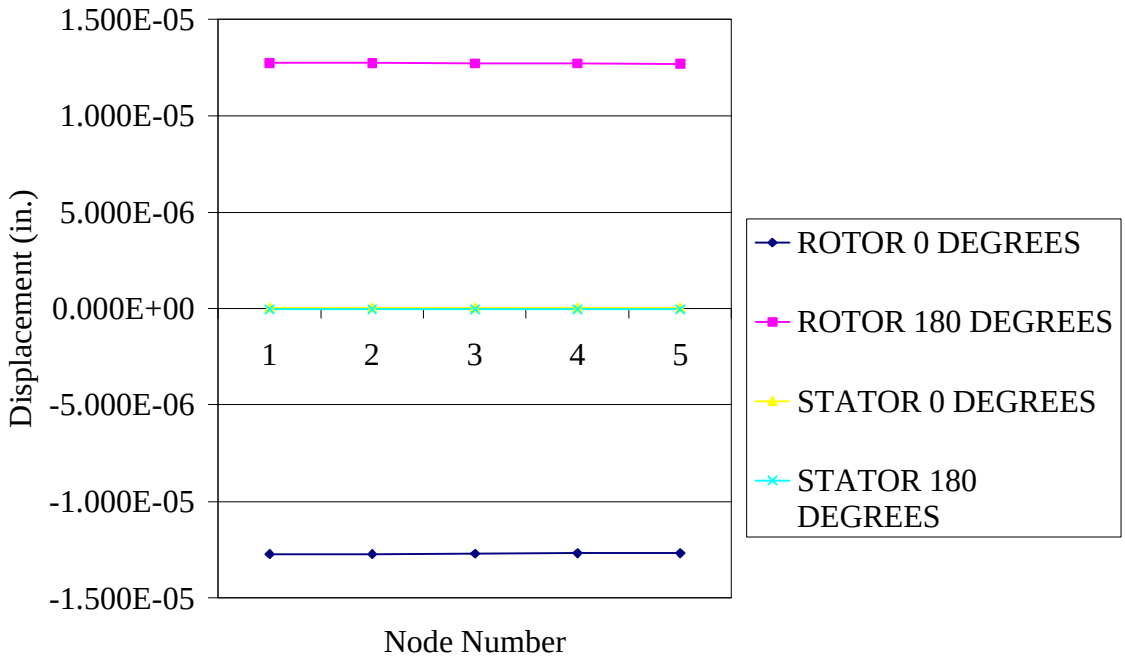

Figure 24. Rotor and Stator Y-axis displacements due to 29.2 Hz force input

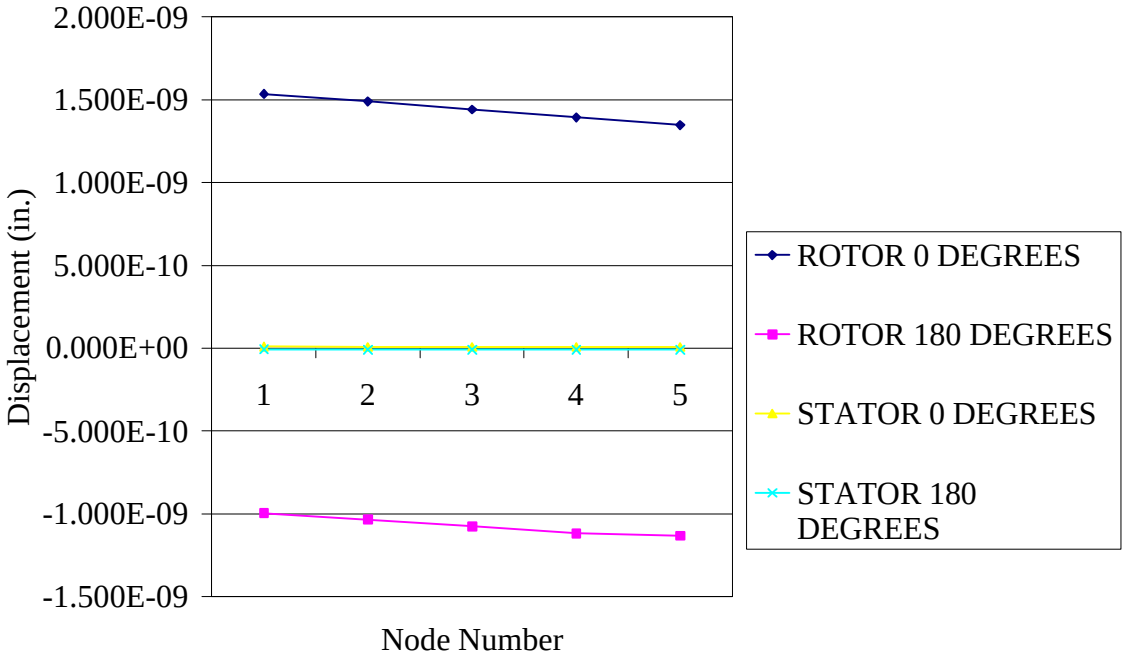

Figure 25. Rotor and Stator Z-axis displacements due to 29.2 Hz force input

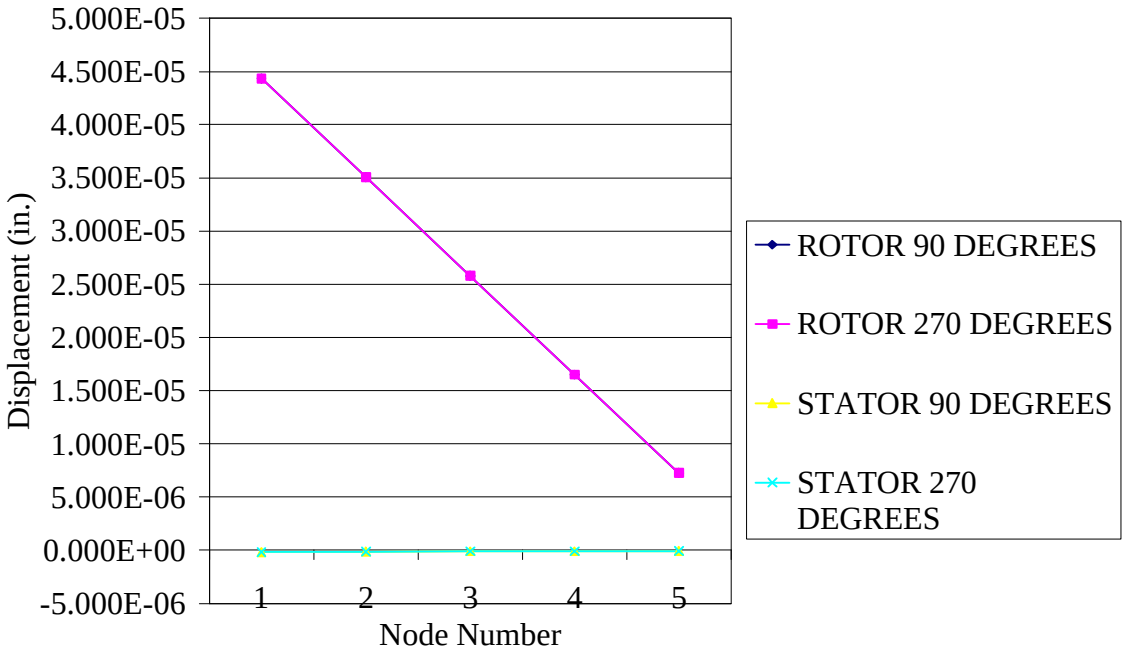

Figure 26. Rotor and Stator X-axis displacements due to 29.2 Hz force input

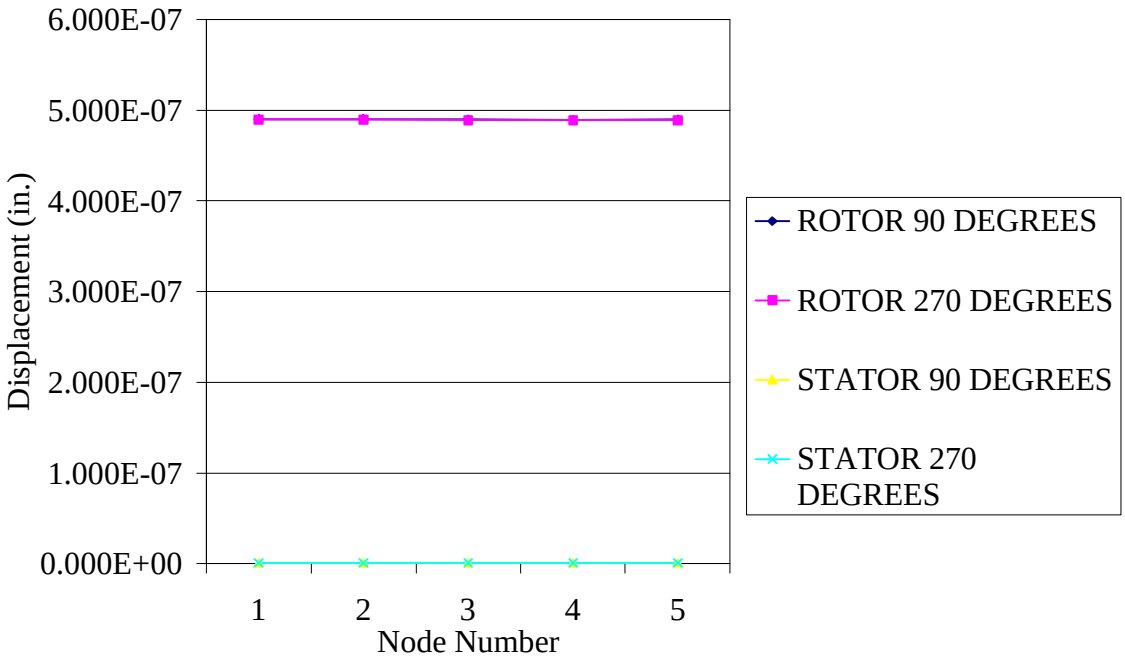

Figure 27. Rotor and Stator Y-axis displacements due to 29.2 Hz force input

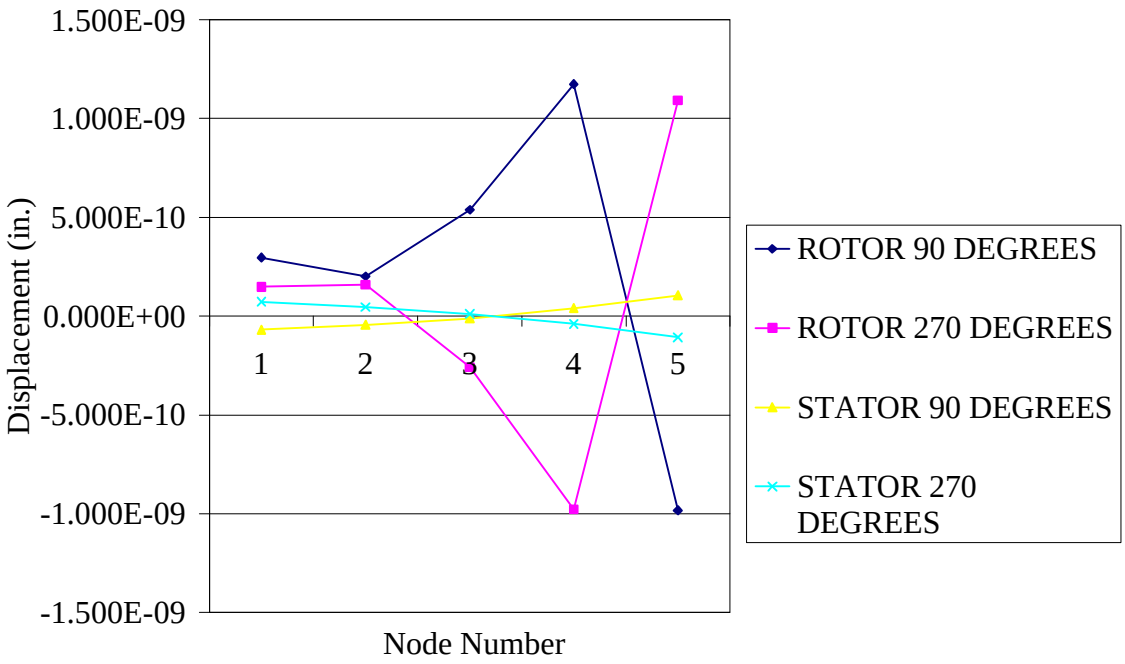

Figure 28. Rotor and Stator Z-axis displacements due to 29.2 Hz force input

The following facts regarding the rotor displacements can be derived from the data.

1) The X-axis displacements at 0°, 180°, 90° and 270° are linear along the rotor length and equal per node for the four radial locations.
2) The Y-axis displacements at 0° and 180° are approximately constant along the rotor length and are equal in magnitude but opposite in sign, respectively. These displacements are of the same order of magnitude as the X-axis displacements and thus are substantial. The Y-axis displacements at 90° and 270° are approximately constant, equal in magnitude and in sign. These displacements are two orders of magnitude less than the X-axis displacements and thus are negligible.
3) The Z-axis displacements at 0° and 180° are approximately linear along the rotor length. These displacements are four orders of magnitude less than the respective X- and Y- axis displacements and therefore may be neglected. The Z-axis displacements at 90° and 270° are not linear and vary from the average value by 46.5 percent. This variation is due to the transition in axial cross-section from rotor to rotor shaft at the rotor bottom. However, these displacements are between four and five orders of magnitude less than the respective X-axis displacements and therefore may be neglected.

From these facts it can be deduced that due to the application of the 29.2 Hz forcing functions the rotor remains cylindrical and thus rigid. Its displacement is essentially two-dimensional in the XY-plane. The rotor is undergoing a clockwise rotation and a translation in the positive X-direction. Thus the rotor shaft behaves as a cantilever beam.

The following facts regarding the stator displacements can be derived from the data.

1) The X-axis displacements at 0° and 180° and at 90° and 270° respectively, are approximately linear. The average X-axis displacement at 0° and 180° is 2.6 percent higher than that at 90° and 270°. This average value is highly biased toward the nodes at the bottom of the stator, where the 0° and 180° displacements are 8 percent higher than the 90° and 270° displacements.
2) The Y-axis displacements at 0° and 180° are approximately constant (less than 1.5 percent average deviation). These displacements are of the same order of magnitude as the respective X-axis displacements and are therefore significant. The Y-axis displacements at 90° and 270° are also approximately constant (less than 0.5 percent average deviation). These are between one and two orders of magnitude smaller than the respective X-axis displacements and are therefore insignificant.
3) The Z-axis displacements at 0° and 180° are approximately linear and are between four and five orders of magnitude smaller than the respective X-axis displacements. These displacements are therefore negligible. The Z-axis displacements at 90° and 270° are not linear and vary from the average value by 63.9 percent. These displacements are three orders of magnitude smaller than the respective X-axis displacements and thus are negligible.

In summary the stator displacement due to the 29.2 Hz force inputs is essentially a two-dimensional problem in the XY-plane. The stator is undergoing a counterclockwise rotation and

is translating in the negative X-direction. This is similar to the situation encountered with the rotor in that the stator and housing are behaving essentially as a cantilever beam. Figures 29 and 30 show the I-DEAS output of the component displacements in the XY (in-plane) and YZ (out-of-plane) planes, respectively. The scales of the displacements in these plots have been increased to 25 percent and 10 percent of the maximum display capability for the XY and YZ planes, respectively, to show the high relative stiffness of the housing/stator assembly in comparison to the rotor/shaft assembly. Because of this large stiffness differential and the small amount of damping used for the system representation, phasing of the displacements between the housing/stator assembly and the rotor/shaft assembly have been neglected.

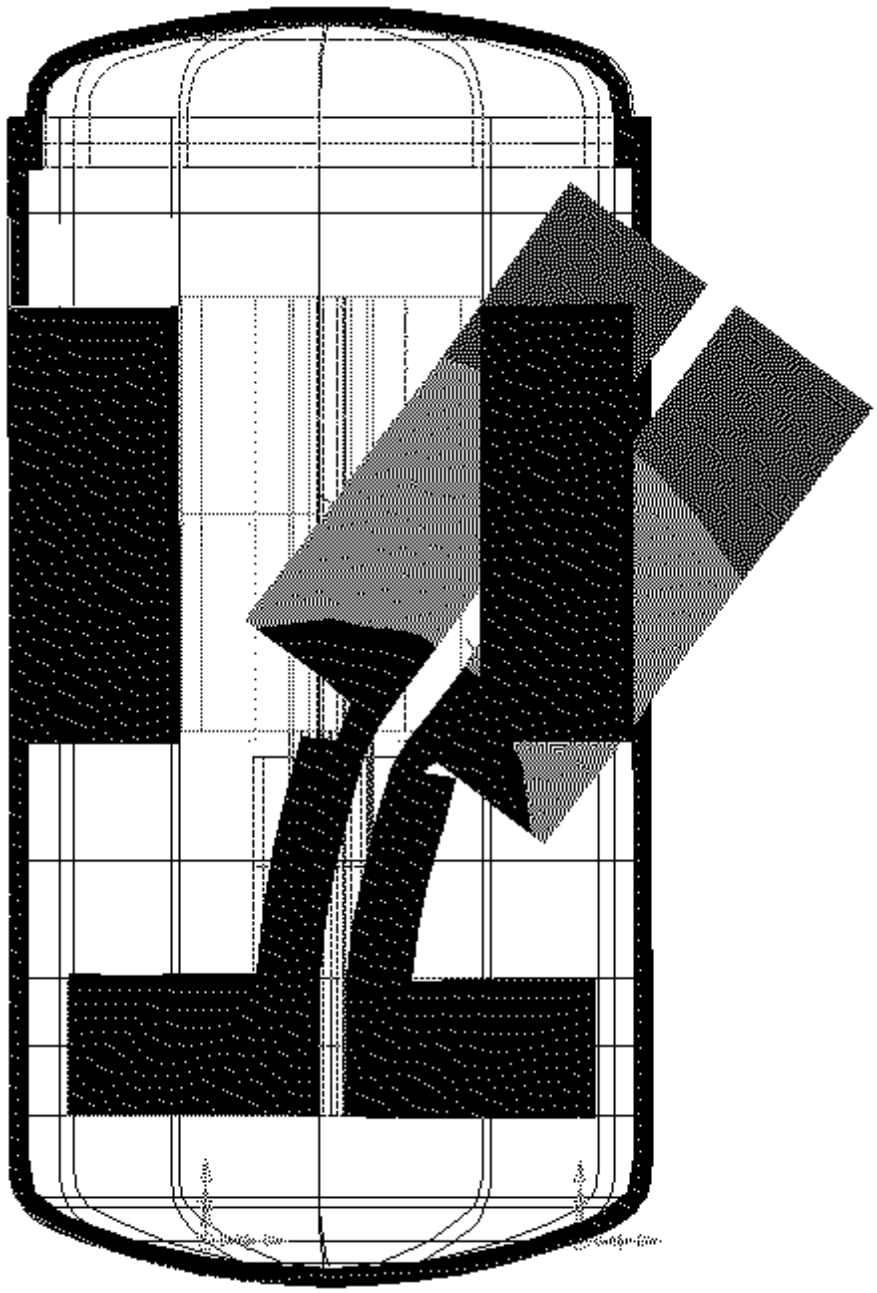

Figure 29. Exaggerated component displacements in the XY plane due to 29.2 Hz force inputs

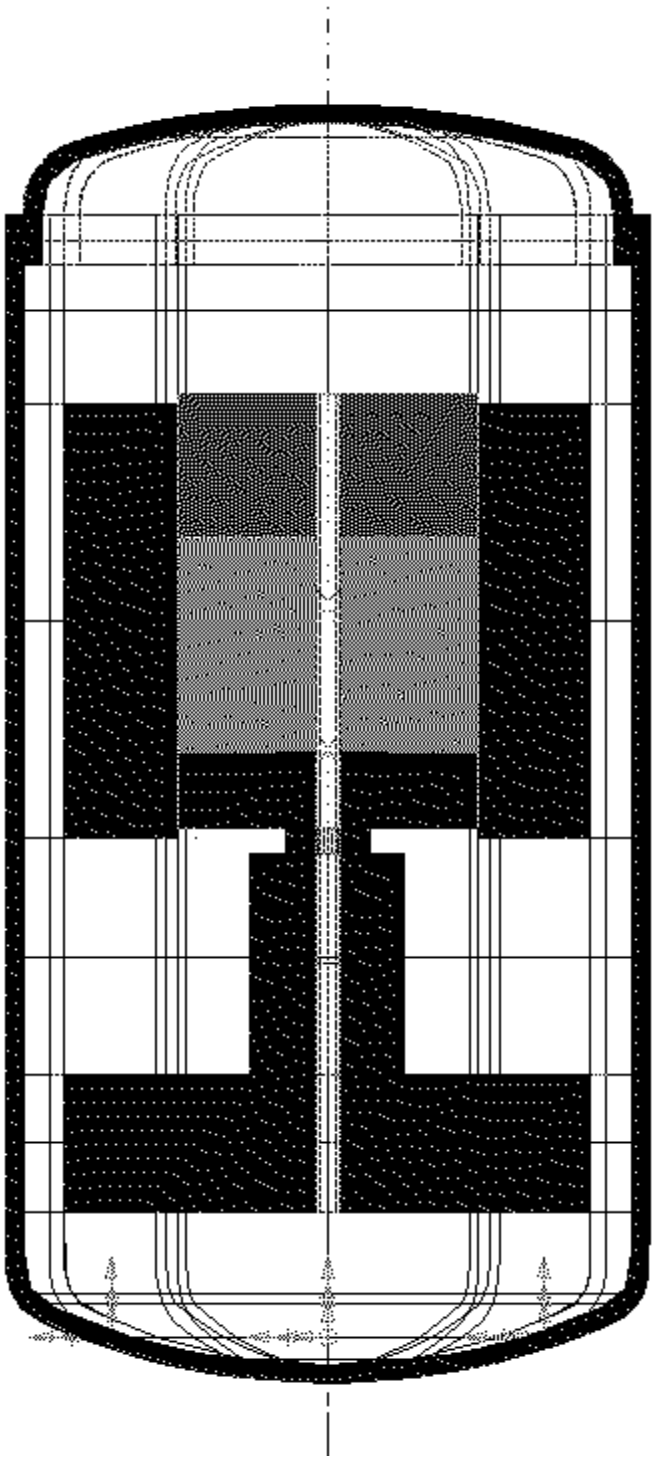

Figure 30. Exaggerated component displacements in the YZ plane due to 29.2 Hz force inputs

5.3.2 Displacements due to 120 Hz input

The rotor and stator displacements due to the 120 Hz harmonic force inputs on the rotor and stator are listed in Tables 12-19 and Figures 31-36 for the 0, 180, 90 and 270 degree locations.

Table 12: Rotor displacement at 0° due to 120 Hz force input on stator and rotor

NODE NUMBER	X DISPLACE. (in.)	Y DISPLACE. (in.)	Z DISPLACE. (in.)
1	5.229 E-05	-1.481 E-05	1.645 E-09
2	4.150 E-05	-1.481 E-05	1.587 E-09
3	3.072 E-05	-1.478 E-05	1.521 E-09
4	1.994 E-05	-1.478 E-05	1.454 E-09
5	9.113 E-06	-1.478 E-05	1.391 E-09

Table 13: Rotor displacement at 180° due to 120 Hz force input on stator and rotor

NODE NUMBER	X DISPLACE. (in.)	Y DISPLACE. (in.)	Z DISPLACE. (in.)
1	5.229 E-05	1.481 E-05	-9.159 E-10
2	4.150 E-05	1.481 E-05	-9.722 E-10
3	3.072 E-05	1.478 E-05	-1.031 E-09
4	1.994 E-05	1.478 E-05	-1.088 E-09
5	9.113 E-06	1.478 E-05	-1.119 E-09

Table 14: Rotor displacement at 90° due to 120 Hz force input on stator and rotor

NODE NUMBER	X DISPLACE. (in.)	Y DISPLACE. (in.)	Z DISPLACE. (in.)
1	5.229 E-05	5.694 E-07	4.034 E-10
2	4.150 E-05	5.692 E-07	2.851 E-10
3	3.070 E-05	5.684 E-07	6.617 E-10
4	1.991 E-05	5.681 E-07	1.385 E-09
5	9.155 E-06	5.685 E-07	-1.100 E-09

Table 15: Rotor displacement at 270° due to 120 Hz force input on stator and rotor

NODE NUMBER	X_DISPLACE. (in.)	Y_DISPLACE. (in.)	Z_DISPLACE. (in.)
1	5.228 E-05	5.687 E-07	2.300 E-10
2	4.149 E-05	5.685 E-07	2.321 E-10
3	3.070 E-05	5.677 E-07	-2.602 E-10
4	1.991 E-05	5.675 E-07	-1.099 E-09
5	9.152 E-06	5.678 E-07	1.265 E-09

Table 16: Stator displacement at 0° due to 120 Hz force input on stator and rotor

NODE NUMBER	X_DISPLACE. (in.)	Y_DISPLACE. (in.)	Z_DISPLACE. (in.)
1	1.362 E-06	-2.025 E-07	2.403 E-11
2	1.227 E-06	-2.027 E-07	2.219 E-11
3	1.091 E-06	-2.023 E-07	2.035 E-11
4	9.520 E-07	-2.015 E-07	1.854 E-11
5	8.097 E-07	-2.014 E-07	1.673 E-11

Table 17: Stator displacement at 180° due to 120 Hz force input on stator and rotor

NODE NUMBER	X_DISPLACE. (in.)	Y_DISPLACE. (in.)	Z_DISPLACE. (in.)
1	1.364 E-06	2.019 E-07	5.444 E-12
2	1.228 E-06	2.021 E-07	3.673 E-12
3	1.092 E-06	2.018 E-07	2.298 E-13
4	9.523 E-07	2.010 E-07	-1.128 E-12
5	8.089 E-07	2.009 E-07	-2.095 E-12

Table 18: Stator displacement at 90° due to 120 Hz force input on stator and rotor

NODE NUMBER	X_DISPLACE. (in.)	Y_DISPLACE. (in.)	Z_DISPLACE. (in.)
1	1.365 E-06	-3.991 E-10	-5.452 E-10
2	1.228 E-06	-4.468 E-10	-4.194 E-10
3	1.092 E-06	-4.545 E-10	-2.641 E-10
4	9.545 E-07	-4.389 E-10	4.460 E-12
5	8.142 E-07	-4.215 E-10	3.916 E-10

Table 19: Stator displacement at 270° due to 120 Hz force input on stator and rotor

NODE NUMBER	**X DISPLACE. (in.)**	**Y DISPLACE. (in.)**	**Z DISPLACE. (in.)**
1	1.365 E-06	-4.040 E-10	5.746 E-10
2	1.228 E-06	-4.518 E-10	4.451 E-10
3	1.092 E-06	-4.596 E-10	2.863 E-10
4	9.545 E-07	-4.440 E-10	1.416 E-11
5	8.142 E-07	-4.266 E-10	-3.762 E-10

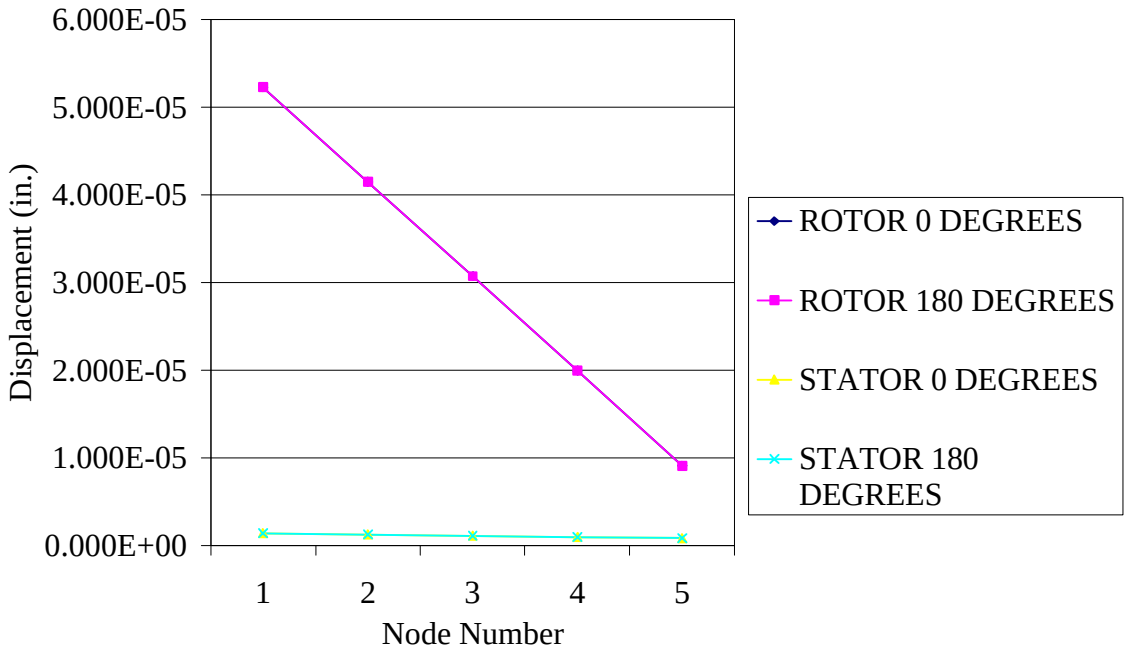

Figure 31. Rotor and Stator X-axis displacements due to 120 Hz force input

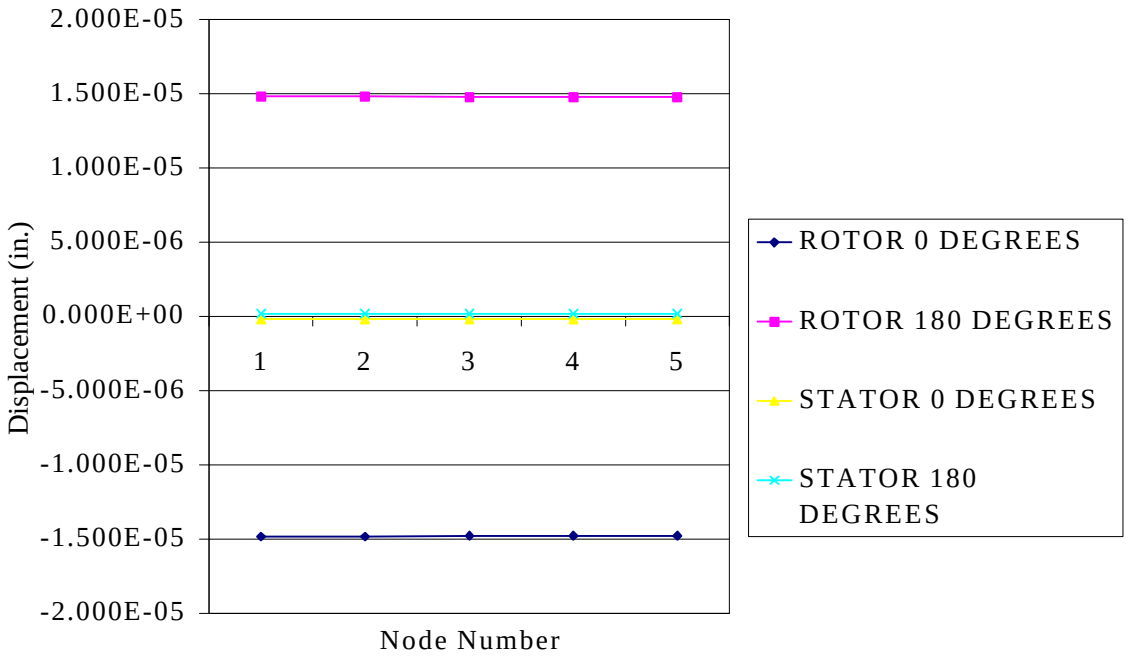

Figure 32. Rotor and Stator Y-axis displacements due to 120 Hz force input

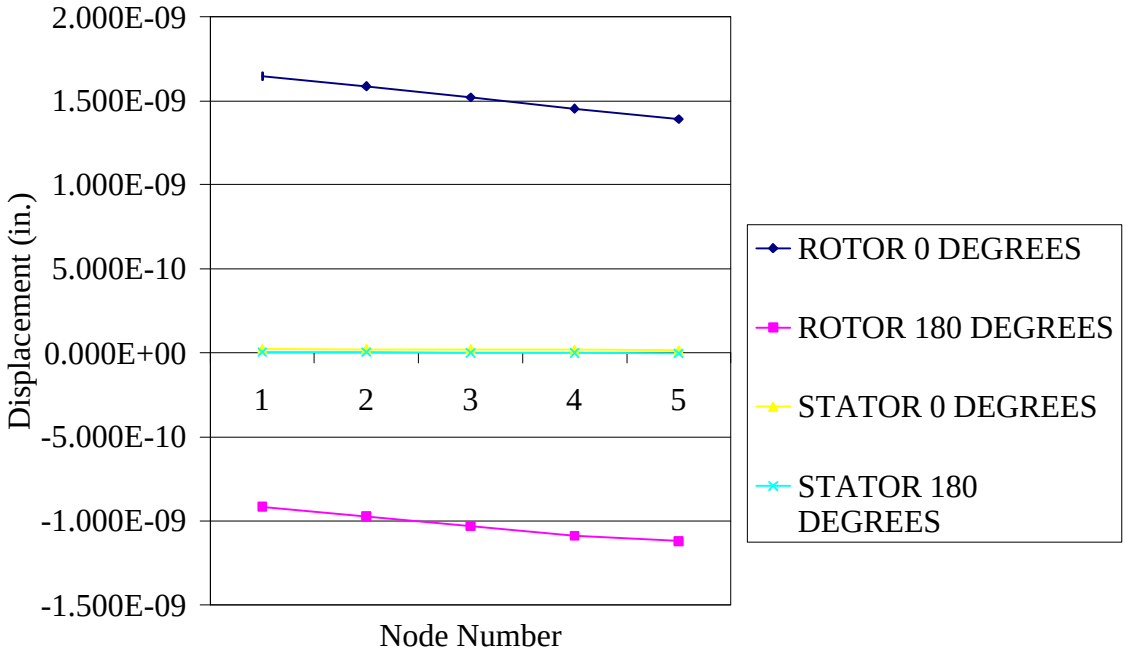

Figure 33. Rotor and Stator Z-axis displacements due to 120 Hz force input

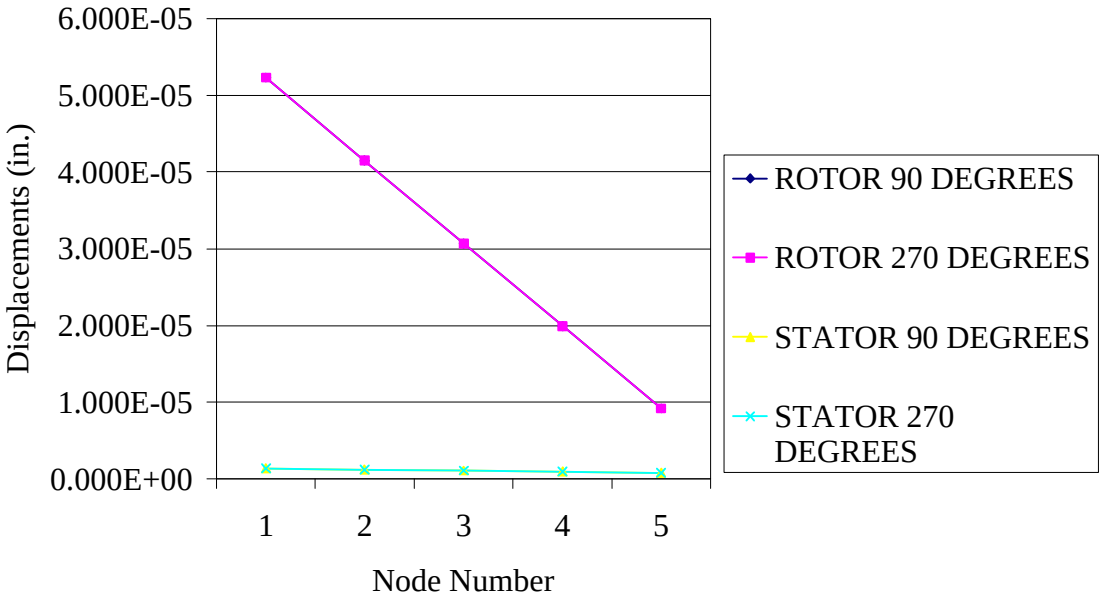

Figure 34. Rotor and Stator X-axis displacements due to 120 Hz force input

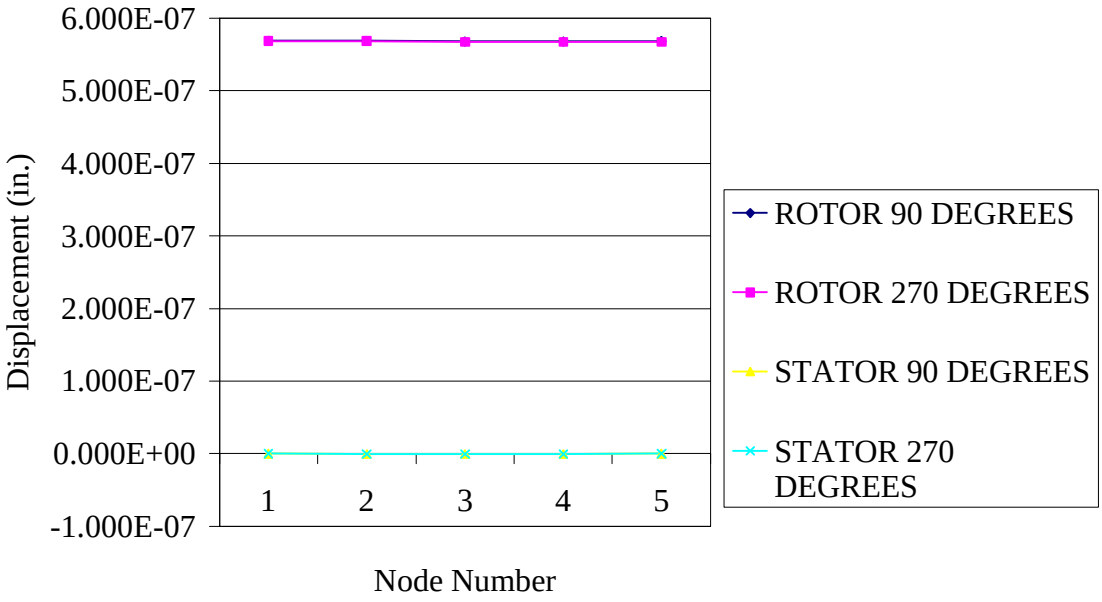

Figure 35. Rotor and Stator Y-axis displacements due to 120 Hz force input

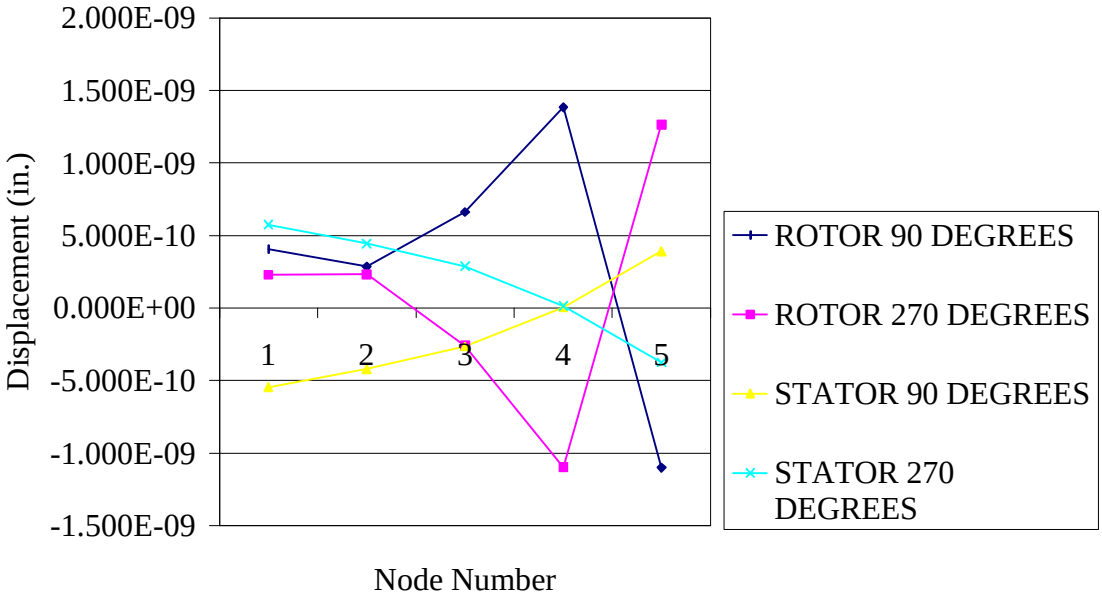

Figure 36. Rotor and Stator Z-axis displacements due to 120 Hz force input

The following facts regarding the rotor displacements can be derived from the data.

1) The X-axis displacements at 0°, 180°, 90° and 270° are linear along the rotor length and equal per node for the four radial locations.
2) The Y-axis displacements at 0° and 180° are approximately constant along the rotor length and are equal in magnitude but opposite in sign, respectively. These displacements are of the same order of magnitude as the X-axis displacements and thus are substantial. The Y-axis displacements at 90° and 270° are approximately constant, equal in magnitude and in sign. These displacements are two orders of magnitude less than the X-axis displacements and thus are negligible.
3) The Z-axis displacements at 0° and 180° are approximately linear along the rotor length. These displacements are four orders of magnitude less than the respective X- and Y-axis displacements and therefore may be neglected. The Z-axis displacements at 90° and 270° are not linear and vary from the average value by 46.3 percent. This variation is due to the transition in axial cross-section from rotor to rotor shaft at the rotor bottom. However, these displacements are between four and five orders of magnitude less than the respective X-axis displacements and therefore may be neglected.

It is obvious that the rotor behaves in virtually an identical manner in response to the 29.2 Hz and 120 Hz force inputs. When subjected to the 120 Hz forcing functions the rotor remains cylindrical and thus rigid. Its displacement is essentially two-dimensional in the XY-plane. The rotor undergoes a clockwise rotation and a translation in the positive X-direction. The difference in the reaction characteristics between the two frequencies is that the rotor displacements due to the 120 Hz forces are greater in all three directions. The maximum X-axis displacement (at the top of the rotor) is 17.9 percent greater for the 120 Hz input. Consequently, the Y-axis displacement at 0° and 180° is 16.3 percent higher for the 120 Hz input.

The following facts regarding the stator displacements can be derived from the data.

1) The X-axis displacements at 0° and 180° and at 90° and 270° respectively, are approximately linear and equal. The X-axis displacements at these four locations are in the positive X-direction. In other words, the stator displacements are in the same direction as the forces applied to the rotor surface and opposite to those applied to the stator surface.
2) The Y-axis displacements at 0° and 180° are approximately constant. These displacements are between zero and one order of magnitude smaller than the respective X-axis displacements and are thus significant. These displacements also follow the same displacement pattern as those on the rotor surface. In other words the 0° displacements are negative while the 180° displacements are positive. The Y-axis displacements at 90° and 270° are not constant. However, these are approximately four orders of magnitude smaller than the respective X-axis displacements and three orders of magnitude smaller than the Y-axis displacements at 0° and 180°. These displacements are therefore insignificant.
3) The Z-axis displacements at 0° and 180° are approximately linear and are between four and five orders of magnitude smaller than the respective X-axis displacements. These displacements are therefore negligible. The Z-axis displacements at 90° and 270° are not linear

and vary from the average value by 64.7 percent. These displacements are between three and four orders of magnitude smaller than the respective X-axis displacements and thus are negligible.

In summary the stator displacement due to the 120 Hz force inputs is essentially a two-dimensional problem in the XY-plane. The difference between these displacements and those encountered due to the 29.2 Hz inputs is that the stator and housing are undergoing a clockwise rotation and are translating in the positive X-direction. Thus the stator and housing are displacing in the same manner and direction as the rotor. Figures 37 and 38 show the I-DEAS output of the component displacements in the XY (in-plane) and YZ (out-of-plane) planes, respectively. The scales of the displacements in these plots have been increased to 25 percent and 10 percent of the maximum display capability for the XY and YZ planes, respectively, to show the high relative stiffness of the housing/stator assembly in comparison to the rotor/shaft assembly. Because of this large stiffness differential and the small amount of damping used for the system representation, phasing of the displacements between the housing/stator assembly and the rotor/shaft assembly have been neglected. While the effect is not great, careful viewing of Figure 37 shows the net positive displacement of the stator and housing due to both force inputs.

5.3.3 Displacement results due to individual force application

At an initial glance the situation described in Section 5.3.2 directly above seems impossible because an object must displace in the direction of the applied force. To assure that the finite element model was behaving correctly analyses were run with the rotor and stator forces applied individually rather than simultaneously. To simplify this segment of the analysis a point load was used on each surface rather than the distributed loads used previously. The moment arm used for this system was the distance between the upper surface of the compression chamber and the mid-length of the rotor. This is not exactly correct because the compression chamber can not be considered true ground. The variation between this moment arm and the true moment arm should be negligible.

The nodal displacement data due to these individual forces can be summarized as follows.

1) All X-axis displacements were linear for both rotor and stator for both applied forces. All X-axis displacements at 0° and 180° were equal in sign and magnitude to those at 90° and 270°. All X-axis displacements were also in the direction of the applied force
2) All Y-axis displacements were analogous to those resulting from simultaneous force application with respect to constant magnitude, linearity and relative order of magnitude.
3) All Z-axis displacements were at least three orders of magnitude smaller than the respective X-axis displacements and thus were negligible. With respect to non-linear displacements of the rotor and stator surfaces all Z-axis displacements were analogous to those found due to simultaneous force application.

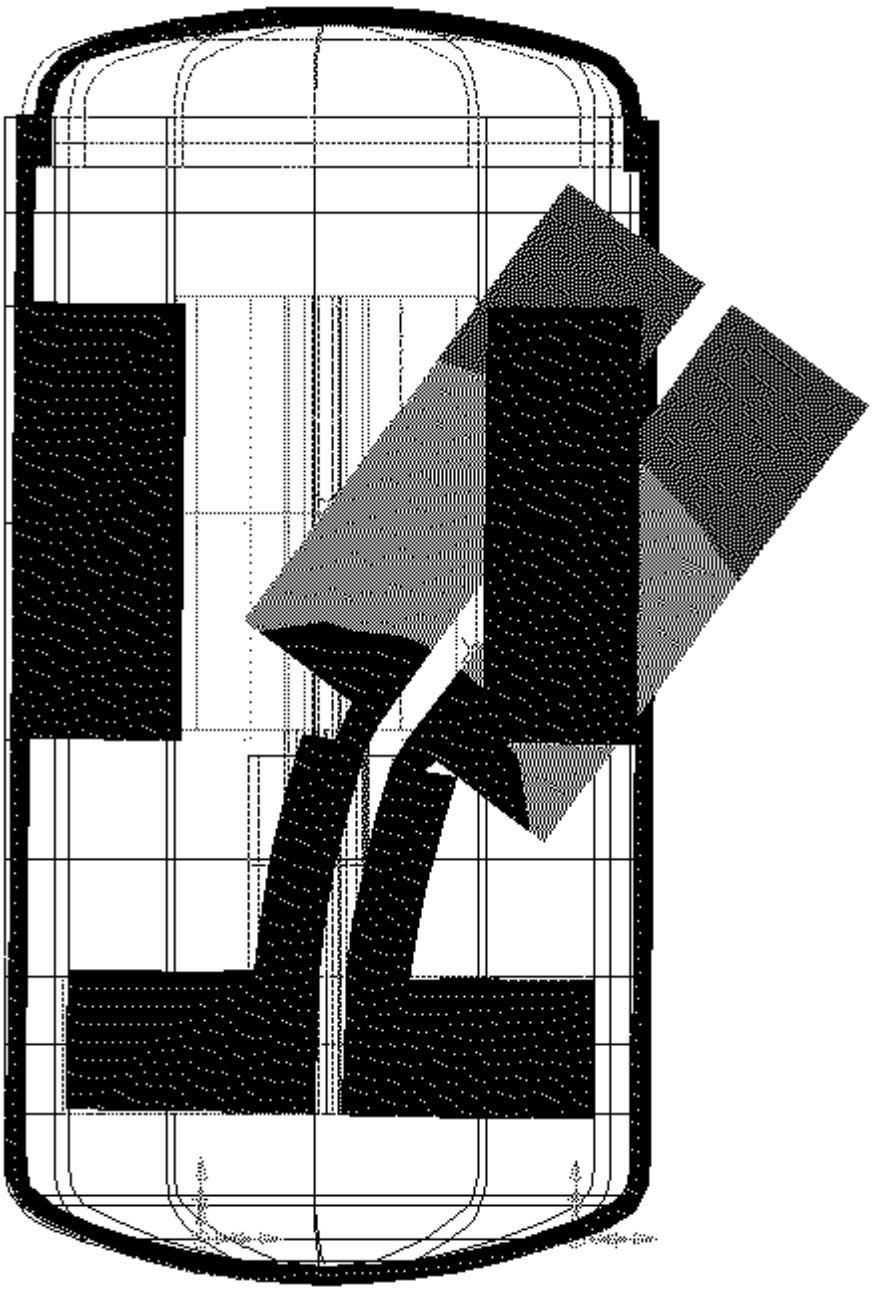

Figure 37. Exaggerated component displacements in the XY plane due to 120 Hz force inputs

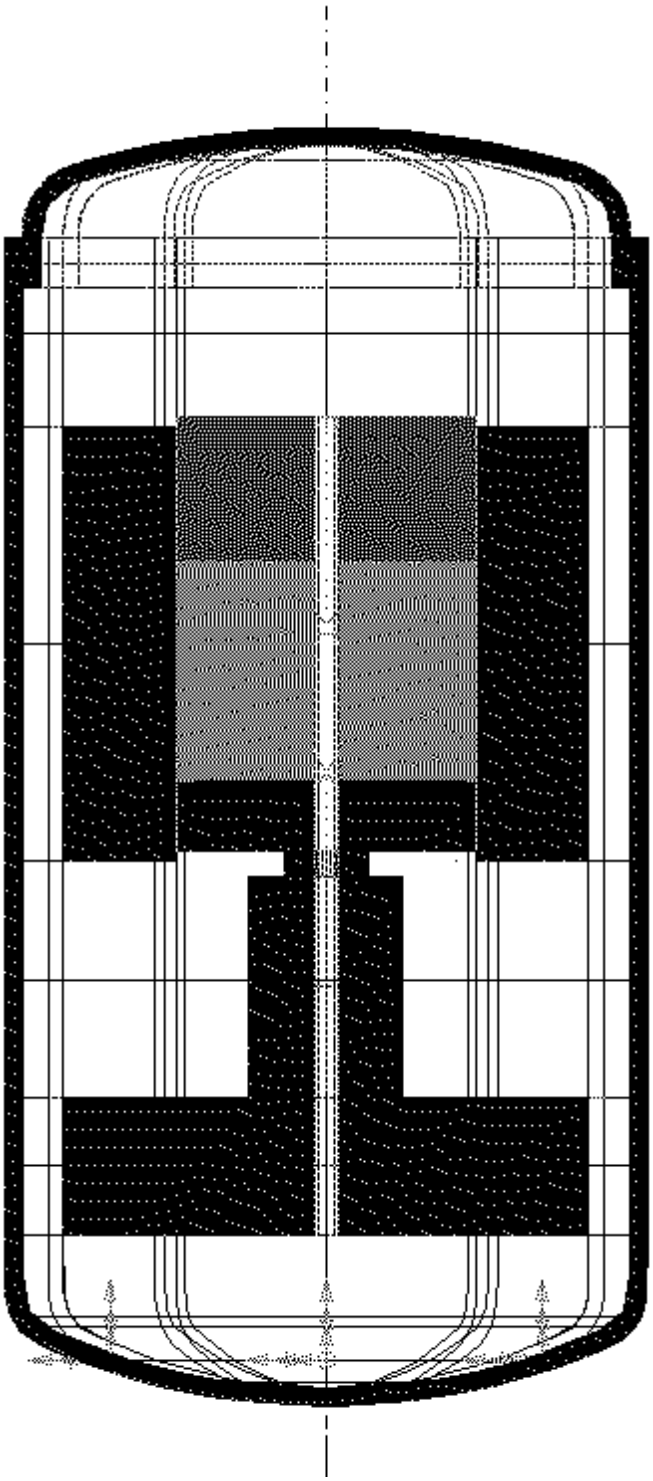

Figure 38. Exaggerated component displacements in the YZ plane due to 120 Hz force inputs

The point to gather from the application of forces individually was that the entire assembly displaces, not just the component directly subjected to the force. In other words the application of a positive X-force on the rotor surface results in positive X-axis displacements of the rotor and stator. This situation is reversed for the stator force. The negative force input results in stator and rotor displacement in the negative X-direction. This phenomenon can be attributed to the energy transfer between the stator and rotor through the housing. This fact explains the positive displacement of the stator during the application of the simultaneous 120 Hz loads. The true scenario is that the positive stator displacements due to the rotor surface force are greater than the negative displacements resulting from the stator surface force. When summed the result is a net positive displacement of the stator.

5.4 Air gap change due to component displacements

As stated the displacements encountered in the system are two-dimensional. With this in mind the following facts can be deduced for both for the 29.2 Hz and 120 Hz inputs, respectively:

1) the horizontal rotor displacement is dominant,
2) the horizontal stator displacement is relatively small but significant and
3) the vertical stator displacement is negligible.

Therefore the change in the air gap can be analyzed by summing the X-axis displacements of the top nodes (Node 1) on the rotor and stator meshes at the 0 degree location and subtracting this quantity from the original air gap of 0.010 in. The results of this analysis are displayed in Table 20. The results due to the simultaneous application of 29.2 Hz and 120 Hz forces are the superposition of the two individual results.

Table 20: Change in air gap due to component displacement

Forcing Frequency (Hz)	Rotor Displacement (in.)	Stator Displacement (in.)	Air Gap Change (in.)	New Air Gap (in.)	Percent Change
29.2	4.435 E-5	-1.798 E-7	4.0 E-5	9.96 E-3	0.40
120	5.229 E-5	1.385 E-6	5.0 E-5	9.95 E-3	0.50
29.2 and 120	9.664 E-5	1.205 E-6	1.0 E-4	9.90 E-3	1.00

In order to produce an interference the change in the air gap must be 0.010 in . This change is two orders of magnitude greater than the interference found due to the simultaneous application of the 29.2 Hz and 120 Hz unit loads on the stator and rotor surfaces. Therefore, if the magnitudes of the applied forcing functions are increased by two orders of magnitude (a 100 lbf input on each surface) an interference should result.

According to Shigley and Mitchell [12] the torque applied to a shaft can be found from the relationship

$$T = \frac{63000H}{n} \tag{5.6}$$

where

T = torque (in*lbf)
H = horsepower
n = shaft speed (rpm)

The shaft torque in an electric motor is equal to the product of the tangential force acting on the rotor and the outer radius of the rotor. Using these relationships and those developed in Chapter 4 between the radial and tangential forces, it can be said that the following is true:

$$H = \frac{p\mathrm{ld}_{\ g}n}{63000} F_{Radial} \tag{5.7}$$

The exact power rating of the electric motor in question was not known. However, it is believed that the motor should be rated at approximately 0.5-1.0 horsepower. The above relationship was used to determine the horsepower rating required to produce an interference. Table 21 lists the required force magnitudes, scale factors and horsepower requirements.

Table 21. Horsepower requirements to produce interference

Forcing Frequency (Hz)	**Radial Force Magnitude (lbf.)**	**Radial Force Scale Factor**	**Horsepower Required**
29.2	250	2.5 E+2	0.286
120	200	2.0 E+2	0.229
29.2 and 120	100	1.0 E+2	0.114

As can be seen, interference between the stator and rotor is possible if the motor produces at least 0.29 horsepower. If the motor output is much greater as expected, the radial force requirement for interference will drop accordingly.

Chapter 6.0 Conclusions and future investigations

In conclusion, in this project it was found that the motor under consideration could experience interference problems between the stator and rotor if the motor's output power rating is at least 0.29 horsepower. Since this requirement is likely met, recommendations are in order for possible solutions to the interference problem.

The first area to examine would be the quality control aspect of the manufacturing process. As stated initially, the interference problems are occurring on about one-third of the units manufactured. This can lead to the assumption that as certain tolerance levels are approached the eccentricity level that produces interference is realized. It was not known at the onset of this project to what extent, if any, stricter quality control measures had been implemented. However, reduction of the amount of eccentricity present in the units through improved quality may be the most cost-effective initial pursuit.

All remaining suggestions deal with the actual design of the unit. For all practical purposes the displacements encountered with this system are the bending of the rotor shaft similar to a cantilever beam with a transverse load. The two most obvious solutions to this problem are to increase the stiffness of the shaft or to utilize a support at the free end.

The displacement for a cantilever beam is directly proportional to the magnitude and location of the applied load and is inversely proportional to the modulus of elasticity of the material and the area moment of inertia of the beam. Obviously the current use of cast iron as the shaft material does not provide the necessary stiffness. The substitution of steel for the cast iron would increase the modulus of elasticity by approximately a factor of two (30.0 Mpsi for steel versus 14.5 Mpsi for non-ductile gray cast iron). This would, in turn, reduce the lateral displacement of the rotor by approximately one-half.

It may be possible to increase the diameter of the rotor shaft and adjust all other geometric parameters accordingly to increase shaft stiffness. This approach appears doubtful when viewing the cross-section of the actual unit because of the close proximity of the rotor conducting bars to the rotor inner radius.

The option of redesigning the compressor/motor assembly to include a bearing support at both ends is obviously the most absolute method for correcting the interference problem. Because the rotor is located at the end of the shaft inclusion of an additional support would almost guarantee success. However, pursuit of this option would totally defeat the purpose of the cantilever design, which was to minimize cost.

Another possible solution would be to retain the cantilever concept but to redesign the geometric parameters of the motor so that the rotor is much larger in diameter but is axially shorter. This would effectively reduce the moment arm of the system and thus the lateral displacements of the

rotor. This approach has been taken by other compressor manufacturers such as Sanyo in the past and has apparently been successful.

Obviously a complete redesign of the unit is a drastic measure. However, because the power output of the motor is not currently known it cannot be discerned whether changing the shaft material to steel will be a sufficient preventative measure. If the motor output is between 0.5 and 1.0 horsepower as suspected this approach will not be effective. It can be shown that if a steel shaft is used and the least volatile static eccentricity is present, a motor output of 0.57 horsepower would be sufficient to produce interference.

With respect to areas for future investigations, the first item would be to ascertain more precise information regarding the geometric characteristics of the compressor assembly. While the use of mapped meshing is restrictive with regards to the allowable amount of component detail, several items in the current model can be more accurately represented. Another area to examine would be the validity of the assumptions made regarding material properties for the laminated stator and rotor.

It was initially desired to reproduce the dynamic air gap so that it could be viewed using the software. Ideally the cylindrical gap would be restructured as a topographical map so that the peaks and valleys could be easily seen. As was noted the I-DEAS software contains no provisions for producing this kind of output. Future development of this area would be of great benefit for analyzing this and similar problems. This project could be approached in several ways, two of which are:

1) Modify the method attempted for this project to place surfaces through the displaced nodes. This approach may prove to be feasible if the ability to pick nodes in a dense mesh could be improved. It may also be possible to place different elements in separate groups during the meshing procedure. This would provide the analyst with the ability to view displaced nodes on individual surfaces. The potential problem with this approach is whether it will work in conjunction with the *Append* command or whether the group information will be lost during the transfer procedure.
2) Write an external piece of computer code to extract the original node locations and their displacements from the Universal File and transfer this data to coordinates necessary for a topographical map. These new coordinates could possibly be imported into I-DEAS and surfaces fitted to emulate the original and displaced cylindrical surfaces. The new air gap between these surfaces could then be easily inspected.

It would also be wise to perform an experimental modal analysis on an existing assembly to validate the finite element analysis results. Experimental analyses on machines consisting of multiple components such as the compressor featured here are complicated. However, Timar's text [2] contains many valuable guidelines regarding experimental modal analysis on rotating electric machinery.

References

(1) Rai, G.B. 1974. *Air Gap Eccentricity in Induction Motors*. Thesis. ERA Technology Ltd. Leatherhead, Surrey, England.

(2) Timar, P.L., A. Fazekas, J. Kiss, A. Miklos and S.J. Yang. 1989. *Noise and Vibration of Electrical Machines*, Elsevier Science Publishers, Amsterdam, The Netherlands and Akademiai Kiado, Budapest, Hungary.

(3) Ozturk, C.O., A. Balikcioglu, H. Acikgoz and A. Bahadir. 1994. Origins of the Electromagnetic Vibrations in Series Fractional Horsepower Motors. In *ISMA Proceedings Vol. 19 Tools for Noise and Vibration Analysis*, 1103-1114.

(4) Girgis, R.S. and S.P. Verma. 1979. Resonant Frequencies and Vibration Behaviour of Stators of Electrical Machines as Effected by Teeth, Windings, Frame and Laminations. *IEEE Proceedings*, 1446-1454.

(5) Knight, C.E. 1993. *The Finite Element Method in Mechanical Design*. PWS-KENT Publishing Company, Boston, MA USA.

(6) Rao, S.S. 1990. *Mechanical Vibrations*. 2nd ed. Addison-Wesley Publishing Company, Reading, MA USA.

(7) Chuse, R. and S.M. Eber. 1984. *Pressure Vessels The ASME Code Simplified*. 6th ed. McGraw-Hill Book Company, New York, NY USA.

(8) Swokowski, E.W. 1991. *Calculus*. 5th ed. PWS-KENT Publishing Company, Boston, MA USA.

(9) Ramani, A. 1993. *Finite Element Modeling of a Refrigeration Compressor for Noise Prediction Applications*. Thesis. Virginia Polytechnic Institute and State University, Mechanical Engineering Department, Blacksburg, VA.

(10) Thomson, W.T. 1993. *Theory of Vibrations with Applications*. 4th ed. Prentice Hall, Englewood Cliffs, NJ USA.

(11) Cheng, F.-H. 1986. *Applied Strength of Materials*. Macmillan Publishing Company, New York, NY USA.

(12) Shigley, J.E. and L.D. Mitchell. 1983. *Mechanical Engineering Design*. 4th ed. McGraw-Hill Book Company, New York, NY USA.

Vita

Swen Thompson

Swen Thompson was born on August 26, 1968 in Roanoke, Virginia. He was raised in Roanoke and completed high school there in 1986. In June 1990 he received his Associate of Science Degree in Engineering from Virginia Western Community College in Roanoke. In August 1990 Mr. Thompson enrolled in the College of Engineering at Virginia Polytechnic Institute and State University in Blacksburg, Virginia. In May 1994 he successfully completed the requirements for a Bachelor of Science Degree in Mechanical Engineering. After working in industry for one year Mr. Thompson returned to the Mechanical Engineering Department at VPI & SU to enroll in the graduate program.

Mr. Thompson will be completing the requirements for the degree of Master of Science in Mechanical Engineering in May 1997. He is looking forward to beginning a career with Schrader-Bridgeport International, Inc. following graduation.